THE PENNSYLVANIA STATE UNIVERSITY
SCHREYER HONORS COLLEGE

DEPARTMENT OF MECHANICAL AND NUCLEAR ENGINEERING

ENERGY PROFILE AND BUCKLING BEHAVIOR OF BISTABLE PLASTIC COLUMN MEMBERS SUBJECTED TO A LATERAL MAGNETIC FORCE

DANIEL MURT
SPRING 2017

A thesis
submitted in partial fulfillment
of the requirements
for a baccalaureate degree in Mechanical Engineering
with honors in Mechanical Engineering

Reviewed and approved* by the following:

Paris R. Von Lockette
Associate Professor of Mechanical Engineering
Thesis Supervisor

Sean Brennan
Professor of Mechanical Engineering
Honors Adviser

* Signatures are on file in the Schreyer Honors College.

ABSTRACT

In solid mechanics, a bistable structure is a structure that has two distinct states of stable mechanical equilibrium. Bistable structures are useful because they can achieve large structural deformations while only requiring a small amount of force to “snap-through” from one stable position to another. Given this snap-through behavior, bistable designs are useful for things like switches, valves, clasps, closures, and actuators, which require to be kept in one of two well-defined statically stable states for prolonged periods of time. One particularly common bistable system is a compressed column exhibiting buckling behavior in one of two stable positions. This paper investigates the use of hard magnets as a means to effect and manipulate the behavior of a bistable buckling column. Hard magnets, when implemented in a bistable buckling column, can achieve measurable changes in the loading and potential energy of the buckling column as a function of the buckling displacement of the column. Additionally, hard magnets are inexpensive, can be modeled as uniform dipoles, and require no external power supply to affect a bistable response. After running multiple buckling tests that fixed hard magnets to a midsection of an acrylic buckling specimen and at a specified proximity to the specimen in space, it was observed that hard magnets indeed noticeably modified the buckling behavior of the thin column. Specifically, the placement and orientation of the magnets were able to successfully modify the initial stiffness, maximum and critical loads, and the overall work done to the buckling column. Additionally, the hard magnets were found to be able to force buckling into one of two mechanically stable states by manipulating the initial distance between the magnets before buckling occurred.

Keywords: bistable, hard magnets, buckling, snap-through

TABLE OF CONTENTS

LIST OF FIGURES

LIST OF TABLES

ACKNOWLEDGEMENTS

I would like to give special thanks to Anil Erol and Kevin Li for all their help and support in the MACs Lab during my research. I would also like to express my gratitude to Dr. Paris von Lockette for his patience and invaluable guidance throughout this research. Finally, I wish to thank my parents Maria and Tom, my sister Katie, and my brother Patrick, whose constant support inspire me to be the very best I can be.

Chapter 1

Introduction

When studying the mechanical response of engineering materials subjected to various types of loading, one thing that is of particular interest to mechanical engineers is how the amount of potential energy inside the material changes as a function of time, position, or both. When viewing the energy potential inside a deforming structure as a function of the structure's deformed shape, the positions of stability of the mechanical system can be observed as equilibrium points, the local maxima and the minimal potential energy. These equilibrium points can be effectively displayed by the "ball on a slope" analogy [1]. In this analogy, we see that the ball is in a stable equilibrium position when the ball's movement is naturally constrained to a single point by a local potential energy minimum (or potential well). We can also see that a neutral equilibrium position is achieved when the ball's movement is limited to only a flat surface (constant potential energy). Lastly, we observe that a position of unstable equilibrium occurs when the ball is on top of the slope (local potential energy maximum), where any small change in the potential energy of the system will result in the ball rolling back down the slope.

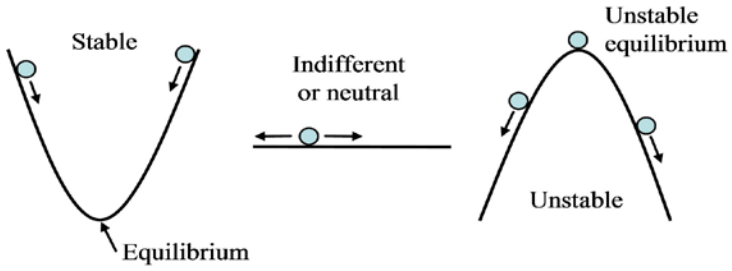

Figure 1. Ball and Slope analogy from Lammers and Zurcher (2011) [1]. Stable, Neutral, and Unstable equilibrium can be visualized as a ball's position on a curved slope. The ball will always return to the bottom of the trough in stable equilibrium, move laterally until static in neutral equilibrium, and fall down the slope at the slightest disruption in unstable equilibrium.

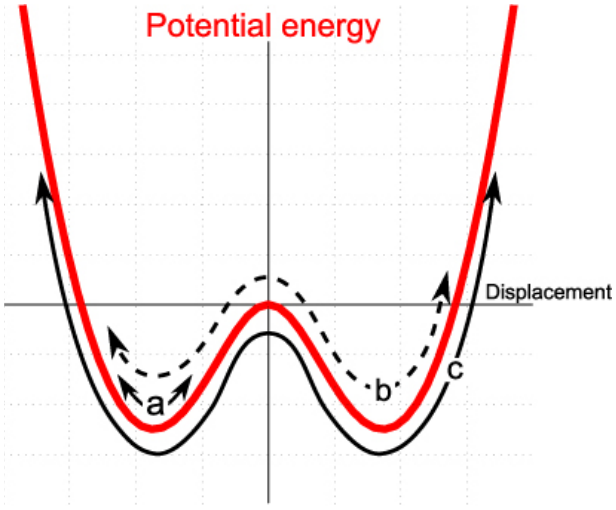

Figure 2. Potential energy distribution of a bistable system adapted from Harne and Wang (2013). Bistability is indicated by two potential energy wells

One specific case of conditional stability that is of interest to mechanical engineers is bistability. Bistable structures have two stable mechanical positions, which can be observed as two distinct local minima in the potential energy curve of the structure [2]. In this example, an unstable equilibrium point separates the two stable energy states of the bistable structure. In order for the bistable structure to switch from one stable position to another, a force must be applied to the structure to push the potential energy up and over the local maximum (unstable equilibrium) and into the other stable (minimum potential energy) equilibrium position. This act of a bistable structure switching between stable positions by overcoming the potential energy hill is called “snap-through.”

Bistable structures are useful because they provide a means to achieve large structural deformations while only requiring a small amount of force to snap through from one stable position to another [3]. Additionally, bistable mechanical designs are useful for things like switches, valves, clasps, closures, and actuators, which require to be kept in one of two well-defined statically stable states for prolonged periods of time [4]. Since bistable structures only

require minimal force to achieve snap through to another stable state, the need for unique methods of actuating bistable structures from one state to another are needed.

This thesis explores the use of magnetic interactions between hard magnets to affect the behavior of a bistable mechanism. The use of hard magnetic interactions to affect bistable behavior is reasonable; hard magnets are inexpensive, require no external power source to operate, can vary in field strength, can be easily adhered to specimens, and can produce a variety of effects based on their orientation with respect to each other. Additionally, hard magnets can behave as a single, uniform dipole and have well-defined analytical behavior that is conducive to simplifying the analysis of their effects on bistable mechanisms.

Specifically, this thesis explores the effects of using hard magnets to affect the bistable behavior of a thin buckling column. The implementation of hard magnets into the buckling column will be used to determine if introducing magnetic attraction or repulsion into the buckling system affects the initial stiffness of the column, the maximum and critical buckling loads of the column, or the energy absorbed by the buckled column over the course of testing. In addition, this thesis explores the degree to which magnetic interaction affects the behavior of the buckling column.

Chapter 2

Background Research

Bistable Mechanisms

Fortunately, the topic of mechanisms that exhibit bistable behavior has been widely studied by mechanical engineers. Some examples of bistable structures include latch-lock mechanisms, corrugated shells, invertible domes, waterbomb shapes, Kresling cylinders, twisted airfoil-like structures, and pre-stressed semi-circular cylindrical shells [3] [5-8]. Simple magnetic dipole interaction can also be used to force bistable behavior in cantilevered beams [4]. The repulsion between each magnet forces the beam into one of two stable positions, creating a bistable system.

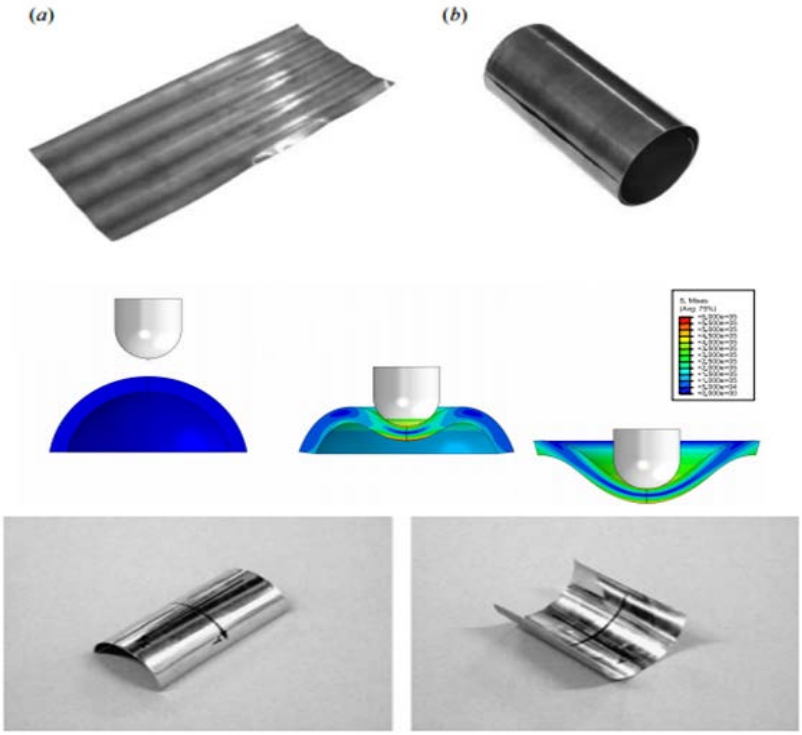

Figure 3. Examples of Bistable Structures. From top to bottom: corrugated shells, invertible domes, pre-stressed semi-circular cylindrical shell. Each structure has two unique positions of stable equilibrium

Another very common example of a bistable system includes a beam in compression that has experienced buckling [9]. After reaching a critical compressive load, a beam will buckle into one of two stable positions. This particular bistable mechanism is important because forced column buckling can be designed such that the buckling-inducing parameters of the system are well defined [10]. For example, the experimenter can directly control the column's elastic modulus, cross-section, length, and end conditions of the specimen to accurately change or predict the critical buckling load of the column. This ability to control the buckling behavior of the column makes the bistable system of a buckled column a good candidate for experimentation. Additionally, the buckling tests are repeatable in a laboratory setting and the response is well understood.

Buckling Behavior

The critical buckling load of a column is dictated by Euler-Bernoulli beam theory, which relates the deflection w, elastic modulus E, and area moment of inertia I of the beam to the beam's bending moment M [10, 11]:

$$M = -EI\frac{d^2w}{dx^2} \tag{1}$$

Assuming a pinned end condition (zero net moment about the beam tip) and summing the moments, we obtain the following differential equation given a load P acting a distance w from the pinned end:

$$EI\frac{d^2w}{dx^2} + Pw = 0 \quad (2)$$

Solving for w using pinned end conditions w(0) = w(L) = 0 (where L is the length of the beam), we get the critical value for load P to induce buckling in terms of E, I, and L:

$$P_{cr} = n\frac{\pi^2 EI}{L^2} \quad (3)$$

The variable n is a coefficient that depends on the end conditions of the beam. In Euler-Bernoulli beam theory, these end conditions include any combination of fixed, free, and pinned ends of the beam. A fixed (or clamped) beam end condition means that there is no lateral translation or rotation about the end of the beam. A pinned beam end condition means that rotation is allowed at the ends of the beam, but not lateral translation. A free beam end condition allows for both lateral translation and rotation at the end of the beam. For any combination of these end conditions, the critical load to cause buckling (called the Euler critical load) derived from Euler-Bernoulli beam theory will change based on the combination [11]. As displayed in Figure 4, the coefficient n in the critical load formula changes according to the end conditions of the buckling beam.

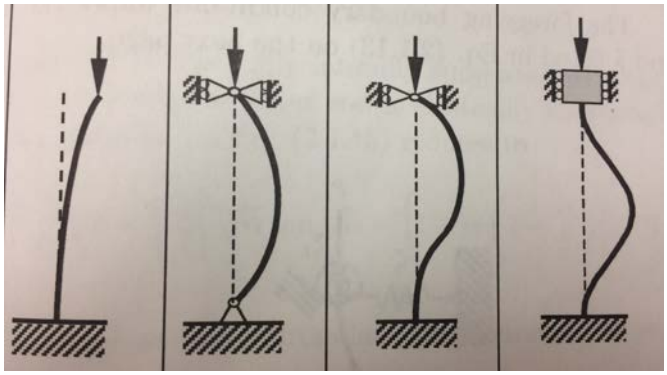

Figure 4. Standard column buckling end conditions in Euler-Bernoulli beam theory from Wang (2005) [11]; From left to right: Free-Fixed (n = 0.25), Pinned-Pinned (n = 1), Pinned-Fixed (n = 2), Fixed-Fixed (n = 4)

Magnetic Dipole Interaction

For any two magnetic dipoles interacting with each other, the potential energy between the two dipoles is described by the equation [12]

$$U_H = \frac{\mu_0}{4\pi}\left[\frac{\overline{m_1}\cdot\overline{m_2}}{r^3} - \frac{3(\overline{m_1}\cdot\vec{r})(\overline{m_2}\cdot\vec{r})}{r^5}\right] \quad (4)$$

where U_H is the potential energy between the two dipoles, μ_0 is the vacuum permeability constant (4π x 10^{-7} N/A^2), m_1 and m_2 are the magnetic moment vectors for each dipole, and r is the vector describing the distance between each dipole. This equation becomes simpler, however, when one considers a case where each dipole has the same magnetic moment vector m, and where both magnetic moment vectors are collinear with distance vector between them. Simplifying, we obtain

$$\pm U_H = \frac{\mu_0}{4\pi}\left[-\frac{m^2}{r^3} + \frac{3m^2}{r^3}\right] = \frac{\mu_0}{4\pi}\left[\frac{2m^2}{r^3}\right] \quad (5)$$

We also observe that the leading constant of Equation (5) depends on the dot products of separation and magnetization of the two dipoles in question. Specifically, the leading constant in Equation (5) depends on parallel and anti-parallel cases shown in Figure 5.

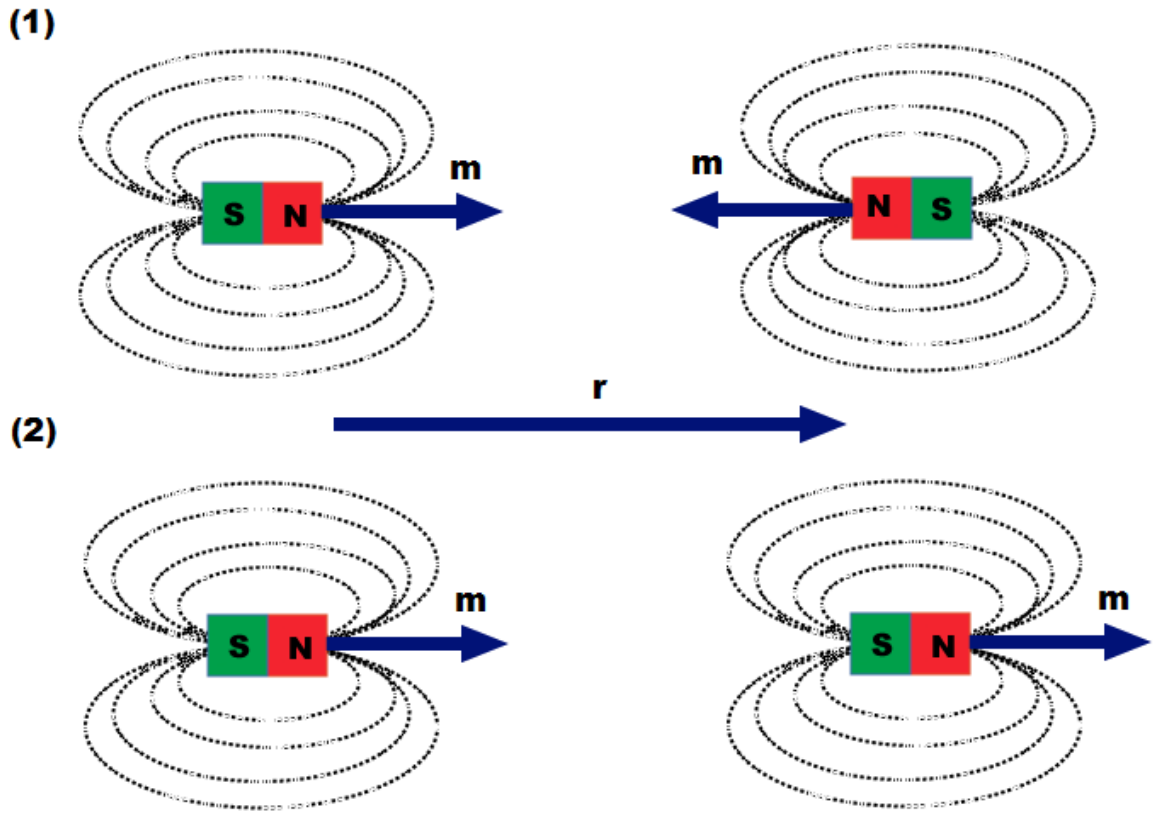

Figure 5. Two collinear cases of dipole interactions. In Case (1), the magnetization vectors m are equal and opposite (repelling). In Case (2), the magnetization vectors are equal and facing the same way as the distance vector r between the dipoles.

To derive the force between two magnetic dipoles, Equation (5) must be differentiated with respect to r (the distance between the two dipoles) [12]. The case shown in Equation (5) where both magnetic moment vectors have the same magnitude and direction sets up the problem for simple differentiation. After performing this differentiation, we obtain

$$\pm\frac{dU_H}{dr}=\frac{\mu_0}{4\pi}\left[\frac{-6m^2}{r^4}\right]=-\frac{3\mu_0}{2\pi}\left[\frac{m^2}{r^4}\right] \tag{6}$$

Like in Equation (5), the leading constant in Equation (6) will change based on the separation and magnetization of the dipoles in parallel and anti-parallel cases. The equations, (5) and (6) will prove useful when analyzing the effect hard magnets have on a bistable system when acting as a single uniform dipole.

Chapter 3

Experimental Methodology

Test Setup Design

Before designing a test setup, a bistable system first needed to be selected for analysis. Given the ease of its testability, a bistable buckling column was the best candidate for experimentation. As previously mentioned, the parameters of a bistable buckling column can be can be explicitly defined by the experimenter to induce a desired critical buckling load [10]. Additionally, buckling behavior can be easily induced by a tensile tester programmed to run compression tests. This effectively allows the force and potential energy inside of the buckling column to be recorded and analyzed in order to observe behavior. The ability to observe the loading and energy inside a buckling column through the use of a tensile tester will also prove to be useful when hard magnets will be used to affect the loading and energy profile of the buckling column.

In order to create a buckling test for analysis, a buckling specimen and a tensile testing machine capable for running compression tests are required. Fortunately, the MACs lab has been recently fitted with the latter: a Shimadzu AGS-X tensile tester. With respect to an appropriate specimen to run column buckling tests on, the specimen must be pliable enough to exhibit smooth, uniform buckling while being thin enough to noticeably experience external magnetic work performed by hard magnets. Additionally, an appropriate column-buckling specimen must be inexpensive and easy to fabricate in quantity in order to have access to many virgin samples for testing. Acrylic, a transparent thermoplastic, met nearly all of these criteria, making it a

suitable candidate for testing. Acrylic is strong, flexible, and cheap to buy in a large variety of sheet thicknesses. Additionally, Acrylic can be easily laser cut to precise shapes and sizes for increased customization. The mechanical properties of acrylic are also readily tabulated for use in calculations of critical loading [13]. One drawback to acrylic is its polymeric mechanical response which includes some degree of viscoelasticity and hysteresis. To overcome these issues, all tests are run at the same compressive rate and buckling results are reported for virgin samples.

The use of thin acrylic for a buckling specimen also lends itself to being easily fitted to the AGS-X for testing. The AGS-X is equipped with two jaw clamps that can hold a specimen in place during testing. With respect to a buckling test, these jaws will simulate fixed-fixed end conditions. These end conditions are explicitly accounted for in Euler-Bernoulli beam theory and will be used to find theoretical critical buckling loads.

The next step in designing an experiment is discerning how to implement hard magnets in such a way to affect the buckling behavior of the bistable acrylic specimen. To begin this step, hard magnets first needed to be selected for testing based on their size, magnetic properties, and utility for this experiment. Based on these criteria, B444 neodymium block magnets from K & J Magnetics were used. These cube-shaped hard magnets are assumed to act as single uniform dipoles (for ease of analysis), but they can also impart up to 4.25 pounds of attractive force when adjacent to each other, despite only being ¼”x ¼” x ¼” in size [14]. Additionally, the small (and well-defined) size of these magnets allows for easy implementation to the bistable buckling column.

In order to implement these hard magnets into the bistable system, the hard magnets must be positioned is such a way so that the magnetic interaction between them affects the buckling

behavior of the column as the cross head of the AGS-X displaces. To achieve this, one hard magnet was placed at the geometric midpoint of the buckling specimen length. Another hard magnet was then fixed in space directly across from the first one at a specified initial distance away. This in effect allows the hard magnet fixed to the buckling column midpoint to interact with the second hard magnet that is fixed in space as the column buckles. The reason that the first hard magnet is attached to the midpoint of the column is due to the shape of the buckling that occurs when both ends of the column are fixed. In this first-mode case of buckling, the column buckles symmetrically with maximum deflection occurring at the column midpoint [11]. It is because of this maximum deflection at the midpoint that the first hard magnet is fixed in the middle of the buckling specimen.

In order to fix the second hard magnet in space, however, additional hardware needs to be used. The first piece of hardware used was a long wooden dowel, to which the second hard magnet would be fixed. Specifically, the hard magnet would be fixed to the end wooden dowel (which had the same diameter as the hard magnet length) with a pole of the magnet directly facing outward. In the interest of convenience, a third hard magnet (that wouldn't be involved in testing) would be fixed to the other end of the dowel with the opposite pole facing outward. Doing this effectively allows the experimenter to switch the outward-facing pole of the second hard magnet by simply rotating the dowel 180 degrees, despite the magnet already being fixed to the dowel. Now that the second hard magnet is fixed to the dowel, the dowel itself must now fixed in space in order to position the second hard magnet directly across from the first. This was accomplished using a ring stand and a ring stand clamp. A ring stand and clamp allows the experimenter to adjust the distance the dowel is positioned above the ground. Additionally, the ring stand clamp allows the experimenter to adjust the distance the end of the dowel is from the

first hard magnet, allowing for customizable initial distances between each magnet before each test. The ring stand also sits snugly beneath the AGS-X top fix its position with respect to the loading frame. Through the use of a wooden dowel, a ring stand, and the knowledge of fixed-end column buckling behavior, hard magnets are able to be effectively utilized to affect the buckling behavior of a bistable acrylic column.

Now that hard magnets have been identified and positioned for use, the dimensions of the buckling acrylic specimen must be determined. In order to achieve an appreciable amount of magnetic work on the bistable buckling column, the critical buckling load of the column must fall in a range such that the force imparted onto the system by the hard magnets can be measured and easily observed by the AGS-X. From Equation (3), the Euler critical load that induces buckling can be lowered by increasing the length of the specimen, decreasing the area moment of inertia of the specimen cross section, decreasing the elastic modulus of the specimen, or by modifying the end conditions of the buckling column. Since the elastic modulus and the column end conditions are already fixed, the specimen length and cross section geometry were the remaining parameters that could be modified to reduce the Euler critical buckling load. Given the ¼” width of the hard magnets, the width of the acrylic specimen was decided to be ½” in order to comfortably fit the hard magnet to the midsection of the acrylic specimen. Due to its availability in the MACs lab, 2-millimeter-thick sheets of unused acrylic would prove to be the best option for raw material with which to laser cut acrylic buckling specimens. Since the width w and thickness t of the buckling specimen have now been decided, the area moment of inertia I of the specimen’s rectangular cross section can now be determined from Equation (7):

$$I = \frac{wt^3}{12} \quad (7)$$

Since the elastic modulus, area moment of inertia, and end conditions are now known, the Euler critical buckling load is now only contingent upon the length of the specimen. For the interactions between the hard magnets on the buckling column to be noticeable, the critical buckling load should be approximately of 20 Newtons of force because the hard magnets can produce up to about 20 Newtons of force between each other. A specimen length of 200 millimeters was chosen because it is not only long enough to directly exhibit obvious buckling behavior, but also has an Euler critical load of 26.74 Newtons, which falls within the expected force range of the hard magnets to exhibit magnetic effects on buckling.

Table 1. Acrylic Buckling Specimen Properties [13]

End Condition Factor (n)	Elastic Modulus (E)	Width (w)	Thickness (t)	Cross Section Area Moment of Inertia (I)	Length (L)
4	3.20 GPa	12.7 mm	2.00 mm	8.47 mm^4	200 mm

Table 2. Hard Magnet Properties from K&J Magnetics [14]

Volume (mm^3)	Brmax (T)	Magnetic Moment (Am^2)
255.64	1.32	0.269

The last part of designing the test setup is addressing the issue of magnet deflection. As the test column buckles, the first hard magnet steadily approaches the second hard magnet fixed to the dowel, which is fixed to a ring stand. In the case where both hard magnets repel each other as the column buckles, the second hard magnet (fixed to the dowel) will be forced to deflect away from the column midpoint, which can affect the work performed by the magnets on the

buckling column. To curb this deflection, a hard wooden frame that could be clamped to the AGS-X was designed so that the end of the dowel could snugly fit through a hole in the frame that would prevent the dowel from deflecting at its end. This effectively allows the hard magnets to get as close as possible to each other in the case the magnets repel each other during buckling.

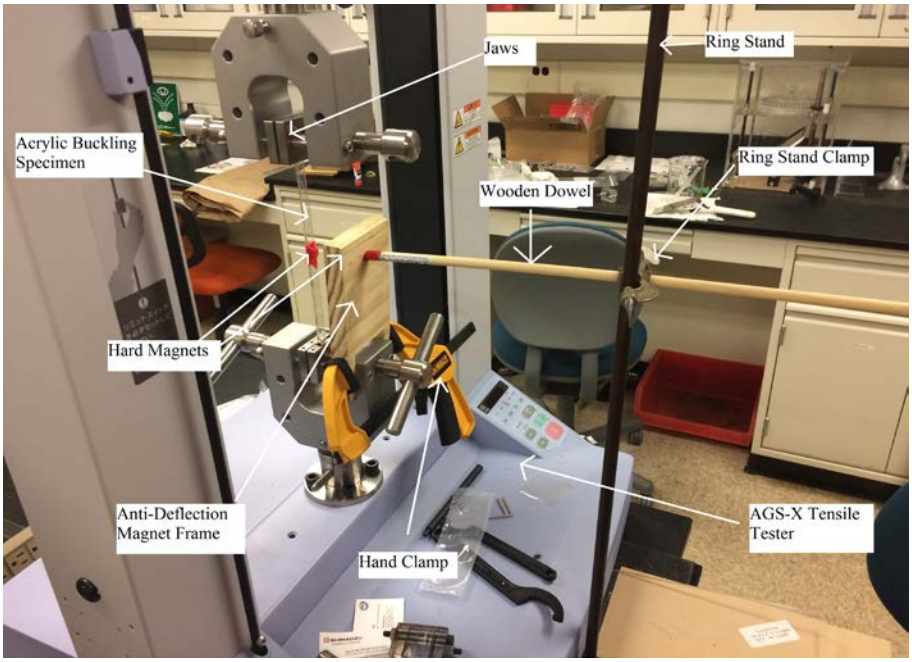

Figure 6. Buckling Testing Setup

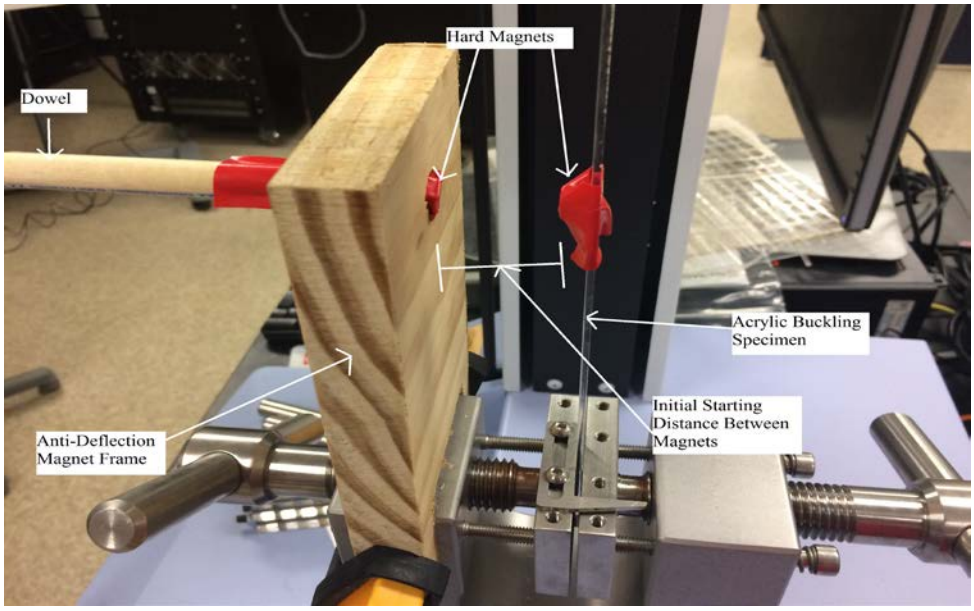

Figure 7. Buckling Testing Setup Close-Up

Testing Procedure

To conduct experiments with the testing setup, 3 different types of buckling scenarios will be investigated: repulsion, attraction, and control cases. For the repulsion case, the hard magnet fixed to the midpoint of the buckling acrylic column will repel the hard magnet fixed in space to the dowel as the column buckles. For the attraction case, the hard magnet fixed to the midpoint of the buckling acrylic column will attract the hard magnet fixed in space to the dowel as the column buckles. For the control case, no magnets will be placed on the buckling column or the dowel. The control case will be used to compare to each of the magnetic cases to observe the effects the magnets have on the buckling column versus when no magnetic interactions are present. The repulsion and attraction cases will serve to display the effect the hard magnets have on the buckling bistable system. Multiple tests for each case will be conducted. Additionally, each case of repulsion and attraction will have a defined starting distance between the first hard magnet (attached to specimen midpoint) and the second hard magnet (fixed in space to a dowel positioned directly across from the first magnet). Since this distance is adjustable, each case of attraction and repulsion will be conducted at starting distances of both 1” and ½”. By manipulating this starting distance between the magnets before buckling begins, the changes in magnetic work performed on the system as a function of initial magnet separation can be better observed.

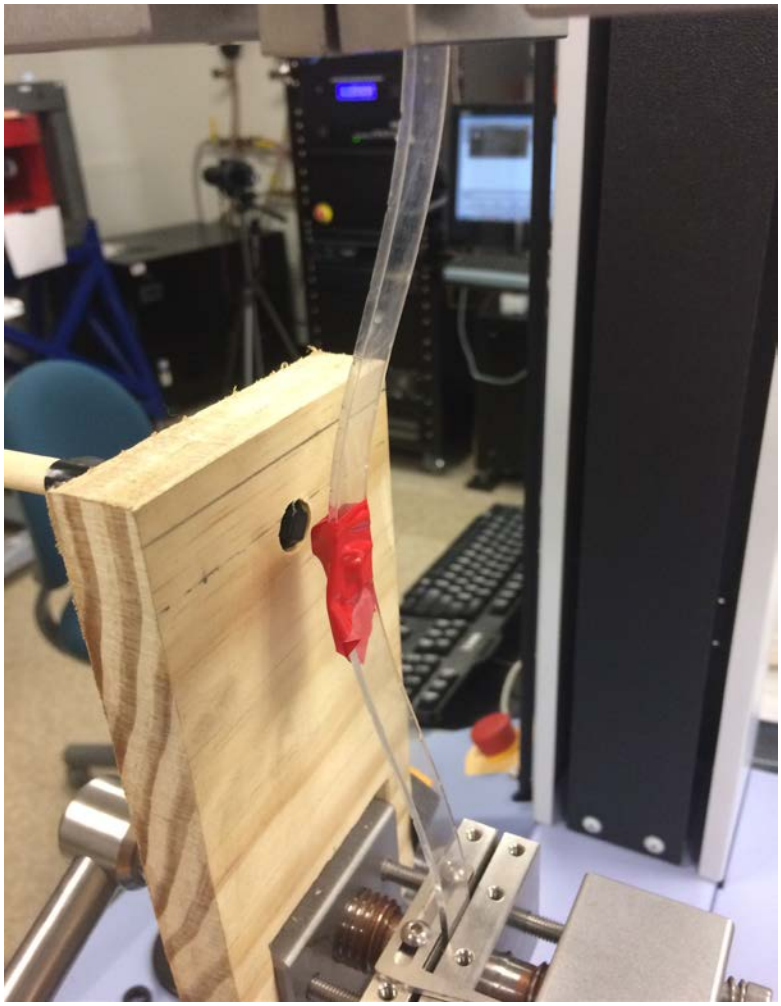

Figure 8. Example of buckling sample being tested (Attraction). Maximum, symmetrical deflection occurs at column midpoint (Fixed-Fixed)

While each buckling test runs, the AGS-X will collect load readings every 10 milliseconds as a function of cross head displacement. To ensure smooth, uniform buckling, the crosshead will displace at 1 millimeter per minute for each case of attraction, repulsion, and control. From the Force versus Displacement graph, the total work performed by the system can be obtained by taking the area beneath the curve graph. Additionally, the AGS-X can calculate slopes, extreme values, and averages across multiple tests. These values will prove to be useful when analyzing the Force versus Displacement data.

Chapter 4

Results and Analysis

The three main parameters that will define that data being analyzed in each test are the magnetic case of the test (repulsion, attraction, or control), the initial distance between the hard magnets in the magnetic cases (1 inch or ½ inch), and the number of testing cycles the specimen has already experienced (first test or last test). Each specimen will undergo a set number of testing cycles and the data that will be analyzed from these tests are the first and last cycles. This will in effect display the differences in behavior from virgin samples and the samples that have already experienced compressive loading. Table 3 shows the names of each test with respect to their magnetic case, initial distance between magnets, and their testing cycle (first cycle or last cycle).

Table 3. Buckling Test Names and Parameters

	First Tests		**Last Tests**	
Initial Distance Between Magnets	**1”**	**½”**	**1”**	**½”**
Magnetic Repulsion	Test 1	-	Test 1	-
	Test 2	-	Test 2	-
	Test 3	-	Test 3	-
	-	Test 4	-	Test 4
No Magnetic Force (Control)	Test 1		Test 1	
	Test 2		Test 2	
	Test 3		Test 3	
Magnetic Attraction	Test 1	-	Test 1	-
	-	Test 2	-	Test 2
	-	Test 3	-	Test 3

Results of Experiments

Overall, there were 6 different groups of test data that were obtained: first control tests, last control tests, first attraction tests, last attraction tests, first repulsion tests, and last repulsion tests. The data for each test group was collected in the form of force versus displacement plots. From these plots, the (repulsive or attractive) interaction between the hard magnets overall displayed some degree of visible effect on the force versus displacement curve of the buckling column compared to the control groups. Of the data collected from each buckling test, the 3 main quantities that were studied were the maximum and critical buckling loads, initial slope of the specimen's force versus displacement curve (stiffness), and the total magnetic and mechanical energies of the buckling system.

After running each group of tests, some noticeable and repeatable differences in force curves began to emerge. Most noticeably, the first (virgin) samples quickly reach a peak force value before the force descends to an asymptotic value, while the last samples did not achieve a peak force value, but rather rose directly to an asymptotic load more gradually than the first test. This can be seen in Figure 9.

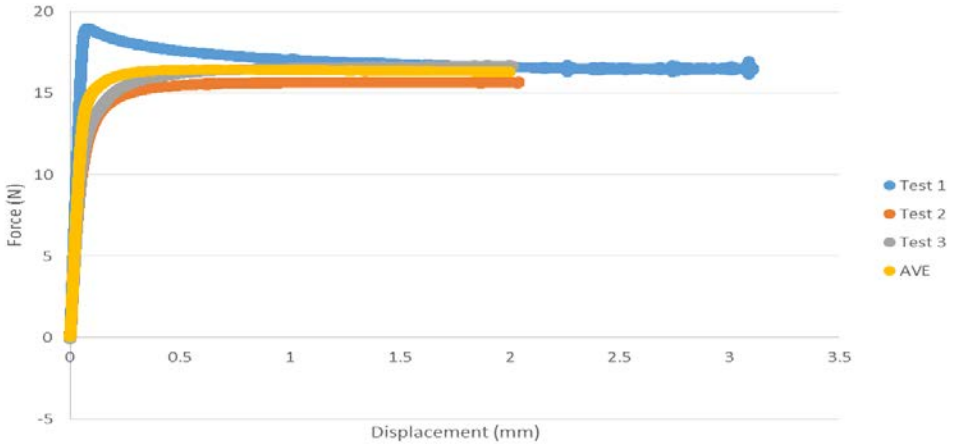

Figure 9. Last Control Tests. Test 1 is the only virgin sample. Untested samples have a sharp force peak and tested samples do not

In Figure 9, Test 1 is a virgin sample while Test 2 and Test 3 are last samples. It is clear from Figure 9 that the first sample achieves a well-defined peak force while Tests 2 and 3 are more rounded and directly achieve asymptotic loading without a well-defined peak force. For Test 1, the maximum force is simply the force at the initial peak of the curve, which is also the distinct critical buckling load. For Tests 2 and 3, however, the maximum force is the asymptotic load since no force peaks are present. Regardless of whether the sample was tested first or last, all tests have initial linear slopes that are measures of the initial stiffness of the buckling column. The values of these slopes are equal to the force in the specimen at the end of curve's linear region (for the virgin samples, these are the peak force values) divided by the displacement of the crosshead of the AGS-X at the end of the curve's linear region.

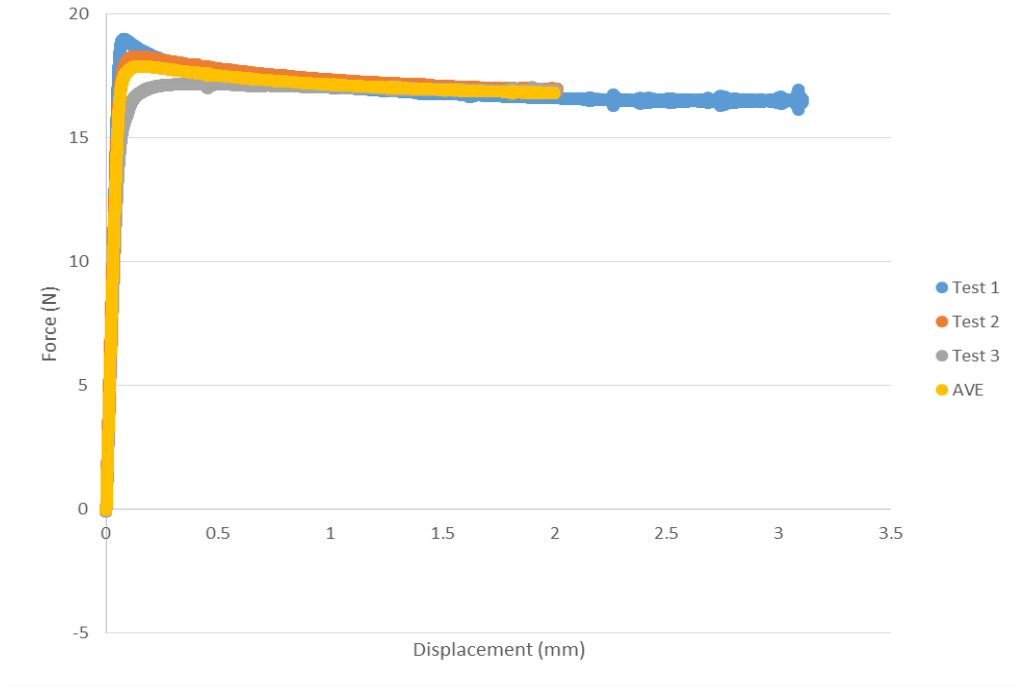

Figure 10. First Control Tests

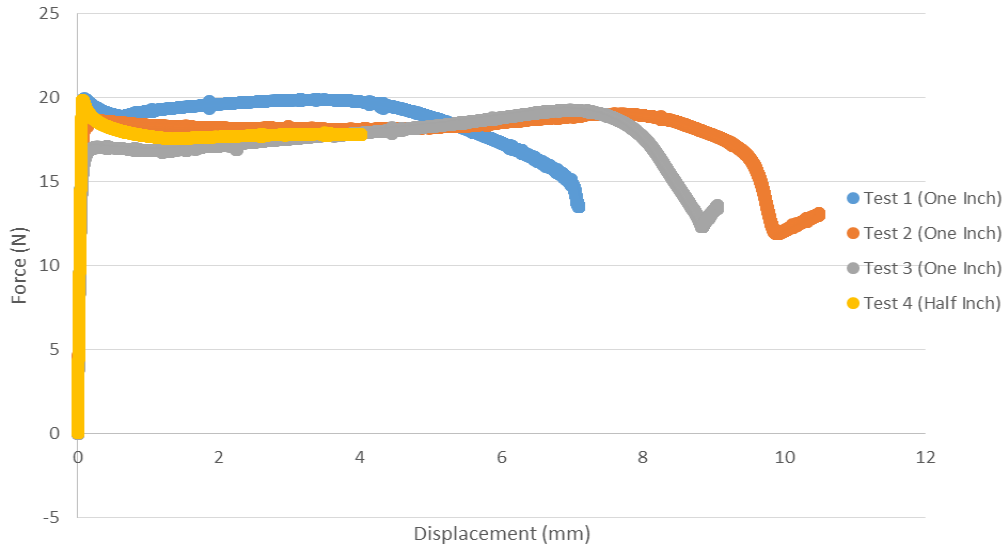

Figure 11. First Repulsion Tests. Test 4 forces buckling into other bistable position and exhibits control behavior

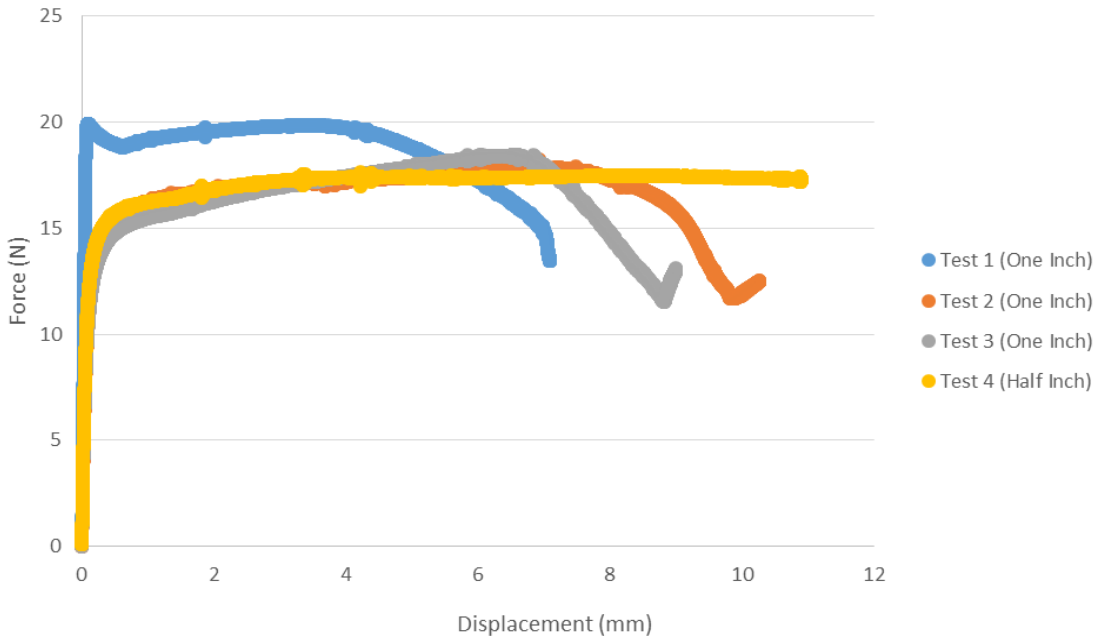

Figure 12. Last Repulsion Tests. Test 4 forces buckling into other bistable position and exhibits control behavior

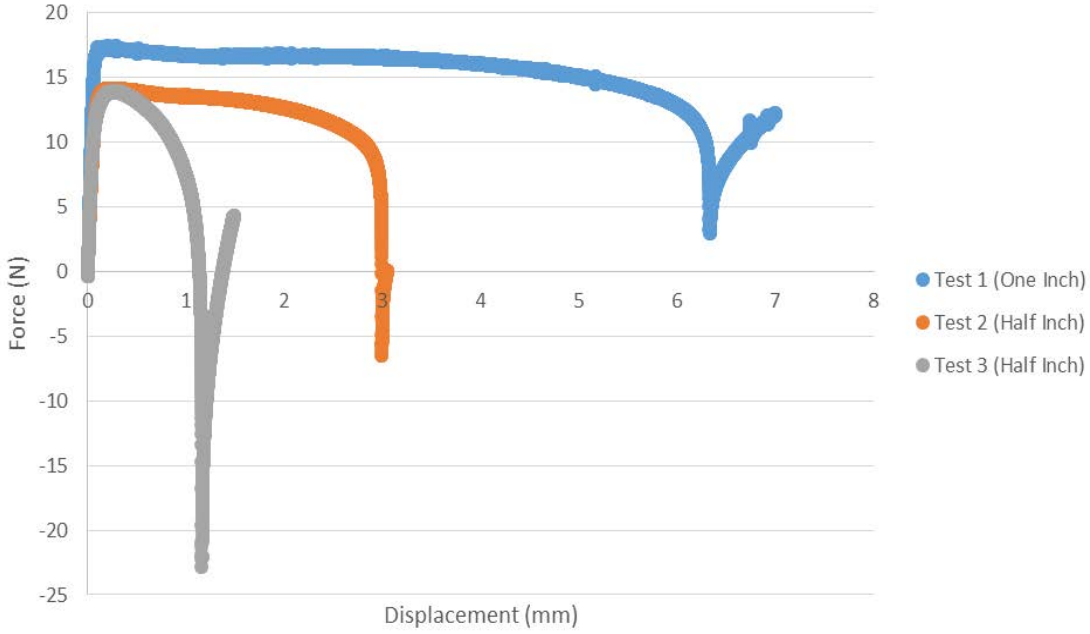

Figure 13. First Attraction Tests

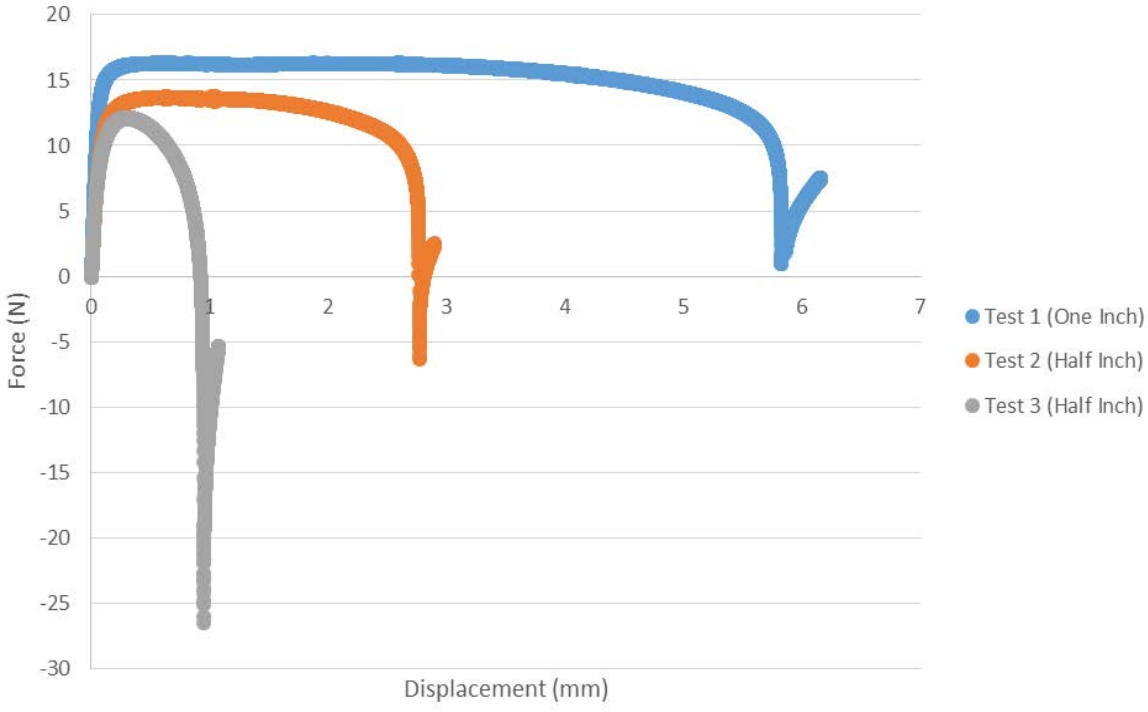

Figure 14. Last Attraction Tests

Table 4. Maximum Loads, Initial Slopes, and Asymptotic Loads for First Tests

		Maximum Load (N)	Initial Slope (N/mm)	Asymptotic Load (N)
Control	Test 1	19.00	330.87	16.58
	Test 2	18.32	307.96	16.95
	Test 3	17.32	220.37	16.92
Attraction	Test 1	17.45	296.25	16.70
	Test 2	14.17	176.77	13.40
	Test 3	13.96	185.90	13.96
Repulsion	Test 1	19.92	206.85	18.89
	Test 2	19.03	283.10	18.12
	Test 3	19.27	220.71	16.71
	Test 4	19.81	266.08	17.77

Table 5. Maximum Loads, Initial Slopes, and Asymptotic Loads for Last Tests

		Maximum Load (N)	Initial Slope (N/mm)	Asymptotic Load (N)
Control	Test 1	19.00	330.87	16.58
	Test 2	15.75	185.70	15.68
	Test 3	16.74	198.47	16.64
Attraction	Test 1	16.31	236.14	16.24
	Test 2	13.78	116.90	13.52
	Test 3	12.11	96.55	12.11
Repulsion	Test 1	19.92	206.85	18.89
	Test 2	18.24	114.40	17.11
	Test 3	18.50	115.59	16.76
	Test 4	17.64	144.77	17.44

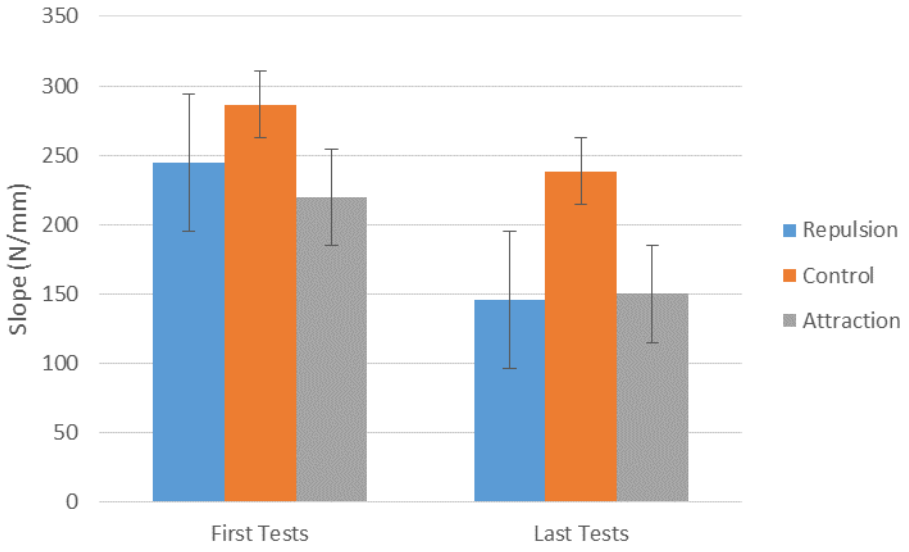

Figure 15. Average Initial Slopes for all First and Last Tests

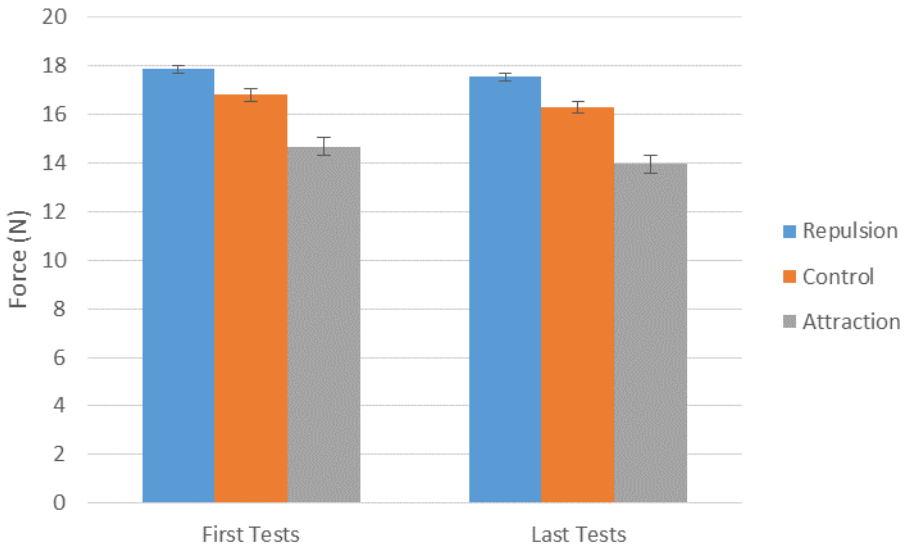

Figure 16. Average Asymptotic Loads for all First and Last Tests

Figure 17. Average Maximum Loads for all First and Last Tests

From the data in Tables 4 and 5, and from Figures 9-16, some general trends can be observed. The first trend that applies across each testing case is that the maximum load, asymptotic load, and initial slopes were all smaller in the last tests than in the first tests. This is due to the fact the mechanical response of acrylic varies due to its viscoelasticity after multiple cycles of testing. From Figure 15, we see that the initial slopes of both the first and last control groups were the largest substantially compared to the repulsion and attraction cases. From Figure 16, we see that the repulsion cases had the largest asymptotic loads, followed by the control and then the attraction cases in both the first and last tests. A similar trend can be seen in Figure 17, where the repulsion cases have the largest maximum loads for both first and last tests, followed by the control and attraction cases. The effect the hard magnets have on the buckling behavior of the acrylic is also apparent in the force-displacement curves of each test. For the repulsion cases, the repelling force between magnets appears to induce an additional force peak in the force-displacement plot in both the first and last tests. The one exception to this can be seen in Test 4,

which looks nearly identical to the control curves. The attraction cases also display a concave-down curve instead of the asymptotic behavior seen in the control curves. Additionally, the curve in the attraction cases appears to become smaller and smaller as the initial distance between hard magnets decreases.

From the collected data, the trends that have been observed appear to have a clear connection to the interaction of the hard magnets with the buckling column. It is likely that the control cases had the largest initial slopes because the initial lateral magnetic force acting on the midpoint of the column in the magnetic cases affected how quickly it took the column to reach its initial maximum load (which affects the initial slope). The repulsion cases likely had the highest average maximum load because (with the exception of Test 4), the column buckled in the direction of the second repelling magnet, whose opposing lateral magnetic force offered slightly more support right before buckling. In Test 4, however, the initial starting distance between the repelling magnets was so close, that buckling was forced into the other bistable position of the buckling column. Since the magnets were then buckling away from each other, there was no more magnetic interaction, thus explaining the shape of the Test 4 curve in the repulsion case. Additionally, the second peak that appears in Tests 1, 2, and 3 in the repulsion case are due to the close proximity of the repelling magnets, causing the load in the column to increase. The attraction cases, however, had the lowest maximum load. This was likely due to the fact that the hard magnet fixed in space in the attraction case never opposes buckling towards itself, causing an inward pulling motion at the column midpoint and thus causing slightly earlier buckling. Similar to the average maximum loads, the repulsion cases had the largest asymptotic loads, followed by control and then attraction cases. The reason for this is also similar to the reason this pattern appears in the maximum loads: buckling in the direction of a repelling magnet offers

slightly more lateral support at the column midsection right before buckling, while buckling towards an attracting magnet pulls at the center of the column and slightly reduces the maximum load at which buckling occurs.

Analysis of Results

To analyze the amount of magnetic work performed on the buckling acrylic column during each magnetic test, we must first determine the total work performed during each test. To accomplish this, we simply take the area beneath the force-displacement curve (integral) for the entire curve. To then find the magnetic work performed on the system, we first take the area beneath the force-displacement curve (integral) for the control case. Since there is no magnetic work being done on the system in the control cases, the work being done to the system is purely mechanical. Then, we take the difference between the total work done during the magnetic case and the total work done in the control case (up to the same amount of crosshead displacement) and the result is the amount of magnetic work performed on the system. The reason this works is because the magnetic cases of buckling experience two kinds of work: mechanical (from the crosshead displacement of the AGS-X) and magnetic (from the hard magnets). Since the identically buckling control case experiences the same amount of mechanical work, the work from the control case can be simply subtracted from the total work of the magnetic case to be just left with the magnetic work.

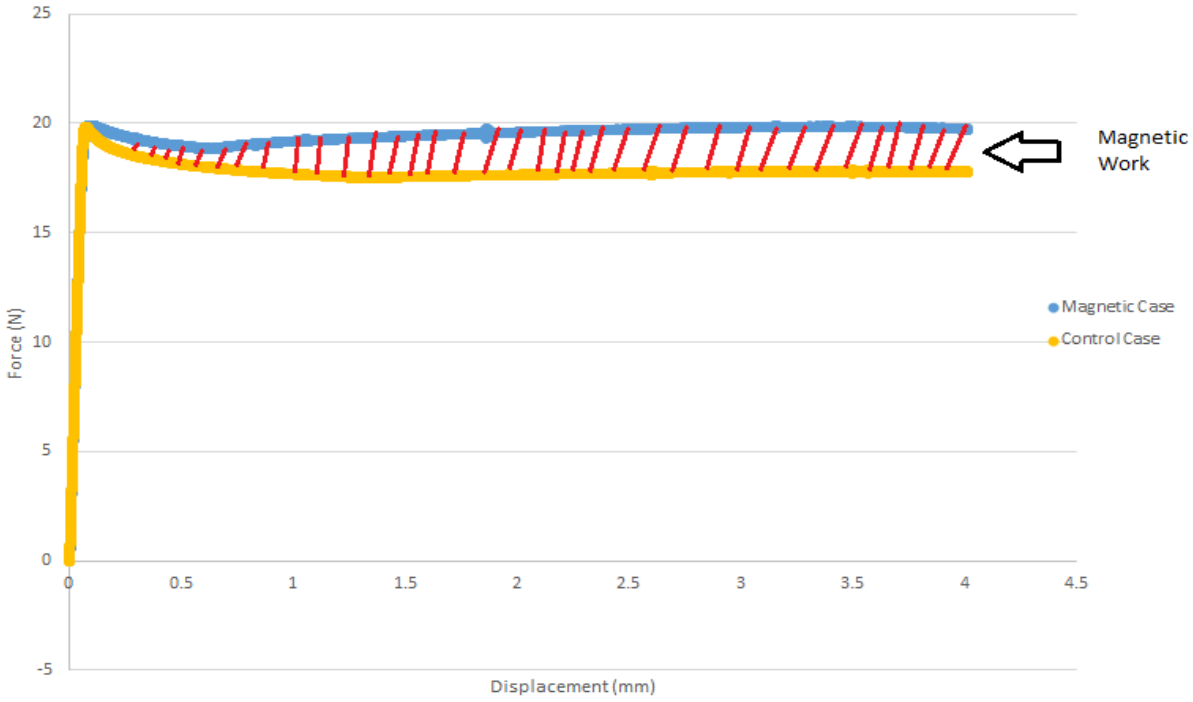

Figure 18. Finding the magnetic work performed in a magnetic testing case. The pure mechanical work of the control case is subtracted from the total work of the magnetic case (mechanical and magnetic) to isolate work done by magnets

Table 6. Mechanical, Magnetic, and Total Work of First Tests

First Tests				
		Total Work (mJ)	**Magnetic Work (mJ)**	**Mechanical Work (mJ)**
Repulsion	Test 1 (1”)	132.59	12.76	119.83
	Test 2 (1”)	173.55	3.48	170.07
	Test 3 (1”)	158.27	5.35	152.92
	Test 4 (1/2”)	70.81	3.02	152.92
Control	Test 1	34.03	0	34.03
	Test 2	33.43	0	33.43
	Test 3	34.41	0	34.41
	AVE	33.96	0	33.96
Attraction	Test 1 (1”)	99.67	18.36	81.31
	Test 2 (1/2”)	37.47	14.11	23.36
	Test 3 (1/2”)	12.36	12.92	0.57

Table 7. Mechanical, Magnetic, and Total Work of Last Tests

Last Tests				
		Total Work (mJ)	**Magnetic Work (mJ)**	**Mechanical Work (mJ)**
Repulsion	Test 1 (1”)	132.59	12.76	119.83
	Test 2 (1”)	159.24	0.31	158.93
	Test 3 (1”)	149.7	6.15	143.55
	Test 4 (1/2”)	65.49	0.80	64.69
Control	Test 1	34.03	0	34.03
	Test 2	30.90	0	30.90
	Test 3	32.12	0	32.12
	AVE	32.35	0	32.35
Attraction	Test 1 (1”)	88.90	5.59	83.31
	Test 2 (1/2”)	34.30	10.26	24.03
	Test 3 (1/2”)	8.77	5.65	3.12

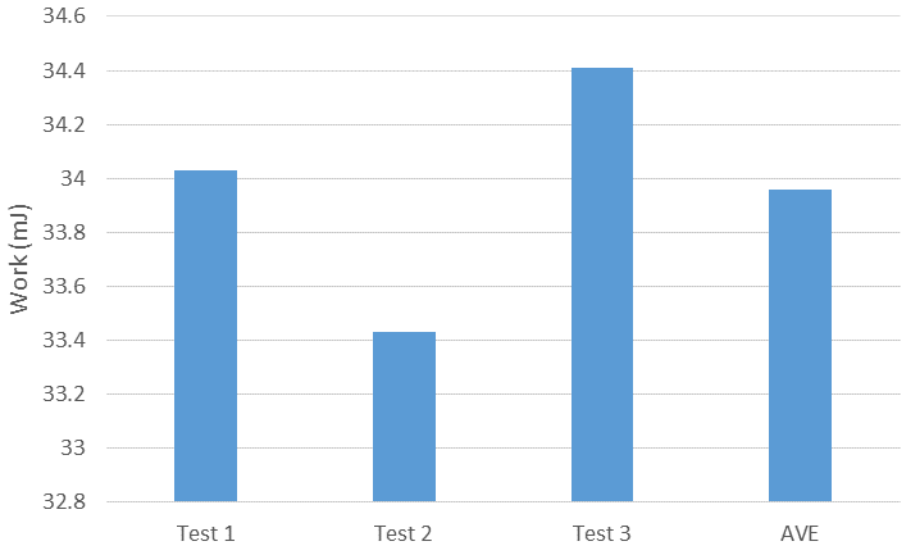

Figure 19. Work performed on First Control Tests

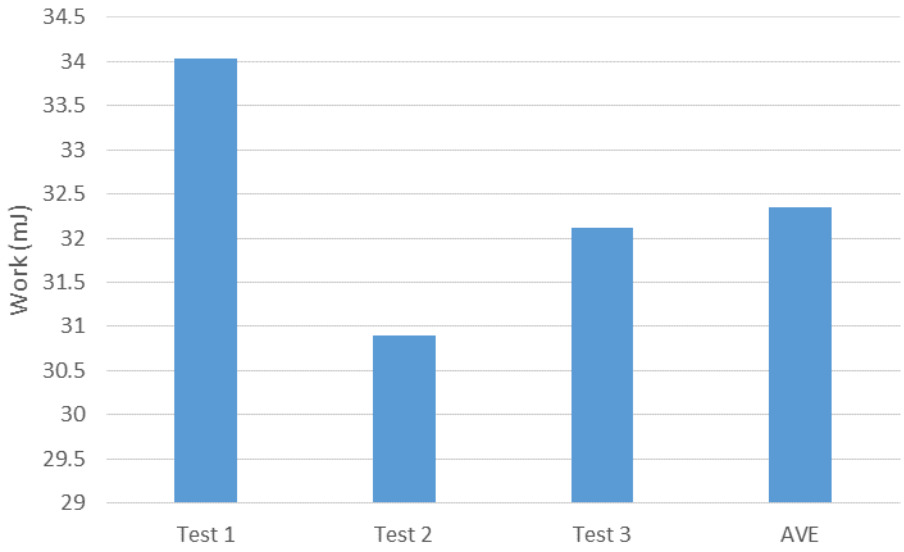

Figure 20. Work performed on Last Control Tests

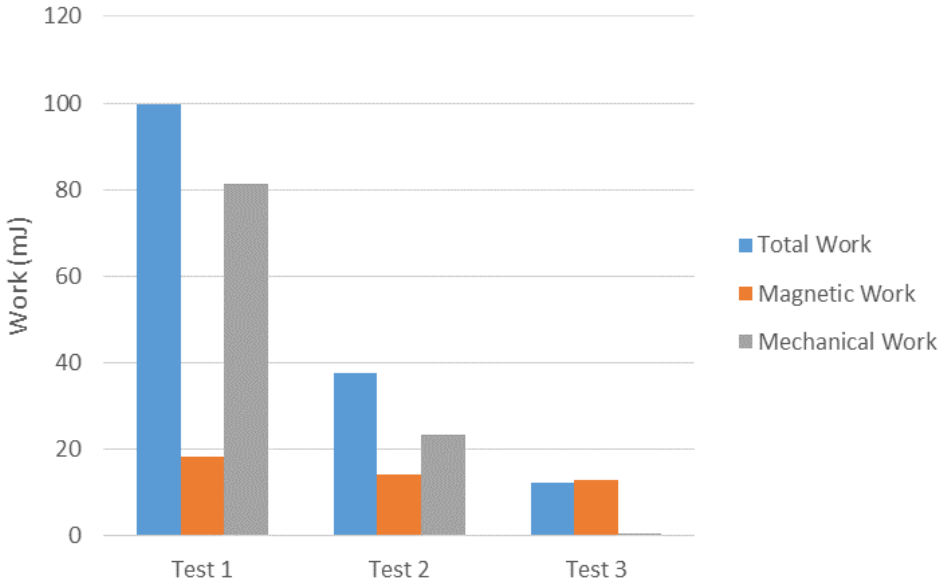

Figure 21. Work performed on First Attraction Tests

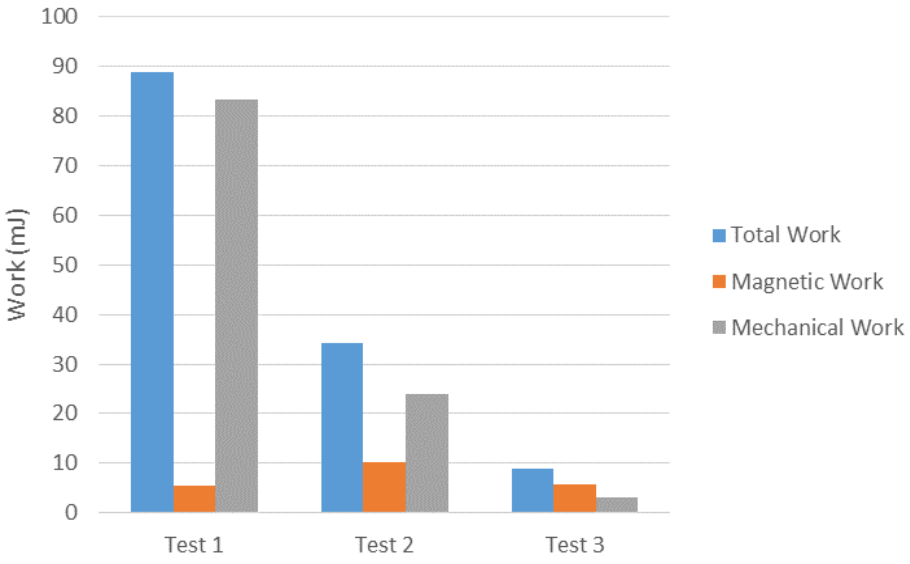

Figure 22. Work performed on Last Attraction Tests

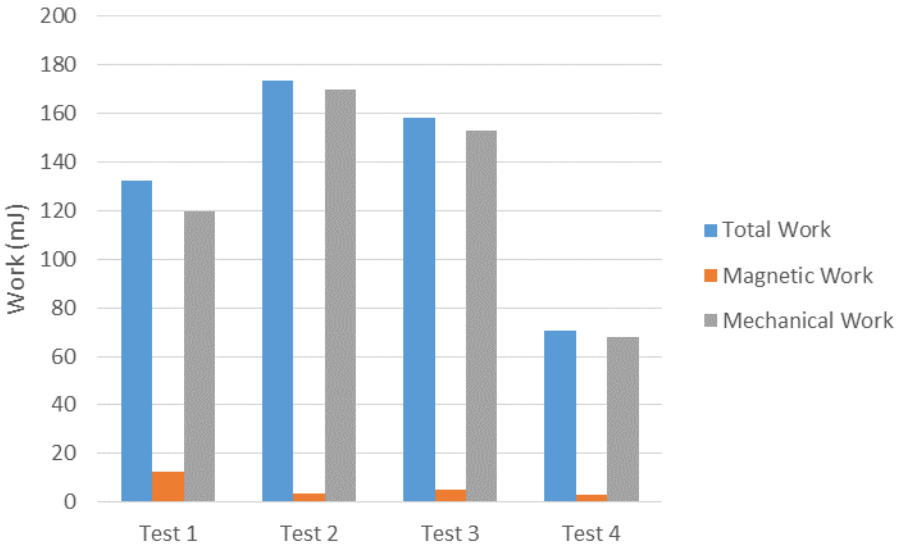

Figure 23. Work performed on First Repulsion Tests

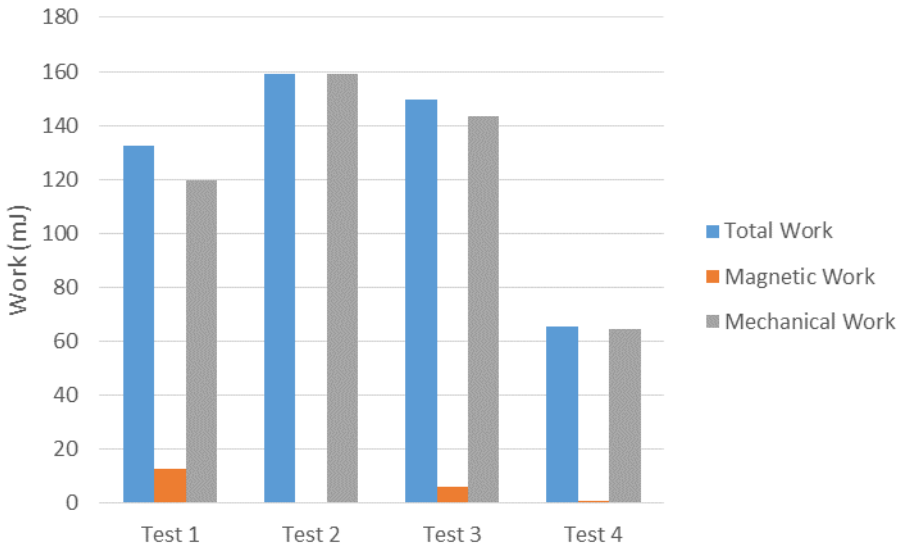

Figure 24. Work performed on Last Repulsion Tests

Across each testing case, we observe that the total amount of work performed during each test is smaller in the last tests compared to the first tests. For most cases, the majority of the work performed on the system is mechanical. However, the attraction tests appear to have the largest percentage of magnetic work being performed on the buckling acrylic. The repulsion cases, however, have a rather small (yet noticeable) percentage of magnetic work being performed on the buckling acrylic compared to the attraction cases. Nevertheless, that small amount of magnetic work was still able to induce a noticeable peak in loading on the column, as seen in Figure 11 and Figure 12 12. In other words, the small amount of work imparted by the repelling magnets to the buckling system was able to effectively modify the loading seen by the acrylic.

The reason for the attraction cases having the largest percentage of magnetic work being performed is likely due to the fact that the amount of mechanical work needed to be performed on the system before the hard magnets made contact was noticeably less in the attraction cases than in the repulsion cases. Additionally, the maximum (critical buckling) load for the attraction cases was observably smaller as seen in Figure 17, due in part by the lateral magnetic attraction influencing column buckling. Another point of observation is that the percentage of total work performed by magnetic interaction in the attraction cases is larger in tests where the initial starting distance between each magnet is ½ inch. When the hard magnets start out this close, the lateral force imparted to the buckling column is greater as the column begins to buckle, thus imparting a larger percentage of magnetic work. Again as with the data gathered in the previous section, the total work performed in each test is lower in the last set of tests than the first set of tests due to the viscoelasticity of the acrylic.

Additional Analyses

From Equation (3) and the data in Table 1, the theoretical critical load for the control cases is

$$P_{cr} = (4)\frac{\pi^2(3.2\times10^9)(8.4667\times10^{-12})}{(0.2)^2} = 26.74\,N \tag{8}$$

A method to calculate the theoretical critical load for the magnetic cases, additional calculation is required. To begin, the buckling column in question needs to be modeled as a vertical buckling column with fixed-fixed end conditions with a lateral spring force acting on the column. The governing equation that determines critical buckling in this case is [11]

$$\sin(d\sqrt{\alpha})\sin[(1-d)\sqrt{\alpha}] - \left(d - \frac{\alpha}{\xi}\right)\sqrt{\alpha}\sin(\sqrt{\alpha}) = 0 \tag{9}$$

In this equation, α represents the critical buckling coefficient multiplied by π^2 (similar to n in Equation (3)), d represents the percentage of the length up the column the force is being applied (d = 0.5 for the midpoint), and ξ is described in Equation (10):

$$\xi = \frac{cL^3}{EI};\ c\ is\ spring\ constant\ with\ units\ of\ \left[\frac{Force}{Length}\right] \tag{10}$$

However, the tests that were run did not apply the lateral force with a spring; the lateral force was applied with two hard magnets acting as magnetic dipoles. To convert the force between two magnetic dipoles to an equivalent spring constant, we must approximate by linearizing Equation (6) via a Taylor series expansion. Taking the Taylor series expansion at a point a, we obtain

$$U_H'(r) = \frac{3\mu_0 m^2}{2\pi}\left[\frac{1}{r^4}\right] = \frac{3\mu_0 m^2}{2\pi}\left[\frac{1}{a^4} - \frac{4(r-a)}{a^5} + \frac{10(r-a)^2}{a^6} - \frac{20(r-a)^3}{a^7} + \frac{35(r-a)^4}{a^8} - \frac{56(r-a)^5}{a^9} + \cdots\right] \quad (11)$$

To linearize, we take the first two terms of the series:

$$U_H'(r) = \frac{3\mu_0 m^2}{2\pi}\left[\frac{1}{a^4} - \frac{4(r-a)}{a^5}\right] = \frac{3\mu_0 m^2}{2\pi}\left[\frac{5}{a^4} - \frac{4r}{a^5}\right] \quad (12)$$

Simplifying Equation (12), we obtain a coefficient for r whose magnitude will serve as our approximated value for c:

$$c \approx \frac{12\mu_0 m^2}{2\pi a^5} \quad (13)$$

In this case, the value of a is simply the initial starting distance between each hard magnet. Plugging Equation (13) back into Equation (10), we obtain a formula for the value of ξ which can then be used to solve for the critical buckling coefficient α:

$$\xi = \frac{12\mu_0 m^2 L^3}{2\pi E I a^5} \quad (14)$$

To calculate the amount of work done to the buckling acrylic solely by the hard magnets, we simply find the negative change in potential energy between the two magnets form the start of the test to the end of the test:

$$Magnetic\,Work = -\Delta U_H = U_{H,1} - U_{H,2} \quad (15)$$

Substituting Equation (5) into Equation (15), we obtain

$$U_{H,1} - U_{H,2} = \frac{2m^2\mu_0}{4\pi}\left[\frac{1}{\Delta r^3}\right] \quad (16)$$

where r is the initial distance vector between each magnet. For an initial distance of 1”, the theoretical magnetic work is 0.883 mJ and for an initial distance of ½”, the theoretical magnetic work is 7.06 mJ, which is closer to the experimentally observed magnetic work done to the system overall.

Chapter 5

Conclusions

In conclusion, the implementation of hard magnets in a bistable buckling column were able to successfully affect buckling behavior. Specifically, the maximum and critical loads, the initial stiffness, and total work of the buckling system were influenced by the hard magnetic interaction.

The maximum loads experienced by the acrylic column were found to increase in the repulsion cases and decrease in the attraction cases by a small but noticeable amount. The initial stiffness of the acrylic column was also observed to follow a similar pattern: the initial stiffness of the acrylic column was found to increase in the repulsion cases and decrease in the attraction cases. Additionally, the viscoelasticity of the acrylic also lead to decreases in initial stiffness as the acrylic samples underwent additional cycles of testing. The hard magnets used to influence the buckling column were also able to successfully impart a noticeable degree of magnetic work to the mechanical work performed by the buckling system: the attraction cases had the highest percentage of magnetic work done on the system while the repulsion cases had the lowest. However, the smaller percentage of magnetic work observed in the repulsion cases was still noticeable enough to produce an additional peak in force in the force-displacement curve, and to force the acrylic to buckle into another stable position away from the hard magnet fixed in space.

Given the overall performance of the magnets in influencing the parameters of a bistable buckling beam, the use of hard magnets may prove effective in the actuation and manipulation of other bistable mechanisms.

Appendix A

Raw Data Plots

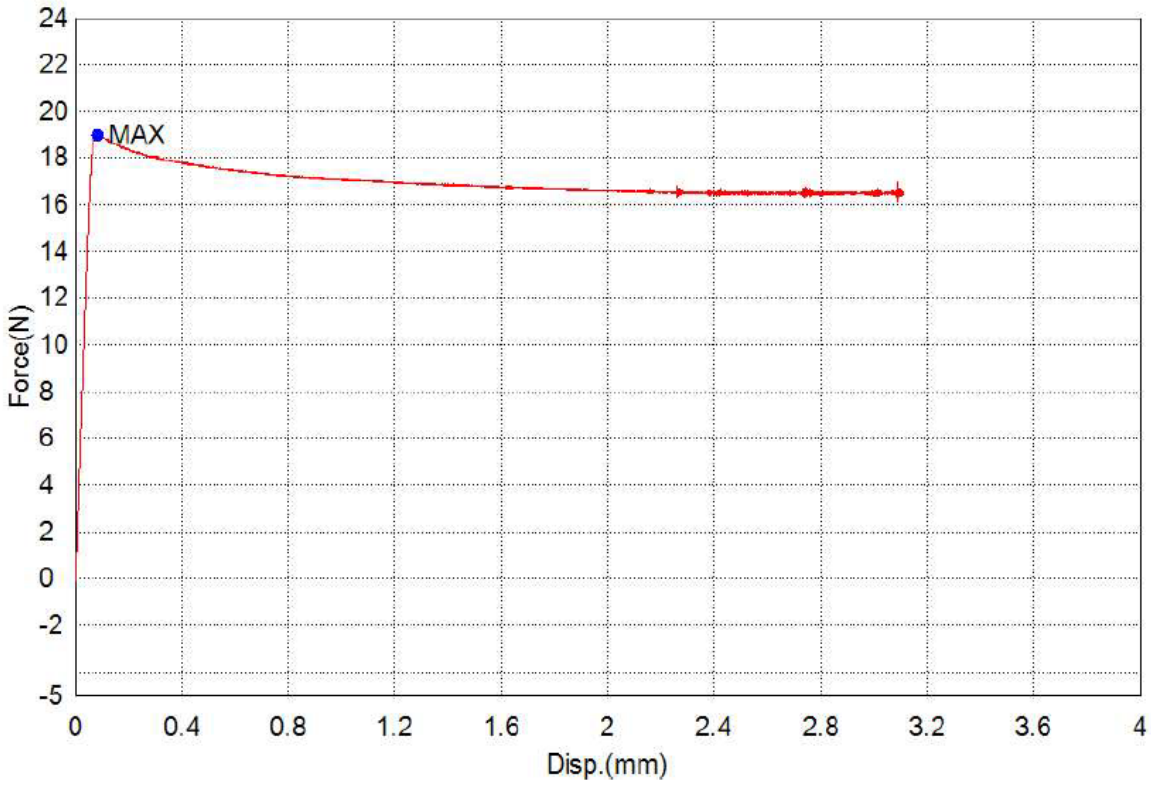

Figure 25. Control Test 1 (1 Cycle)

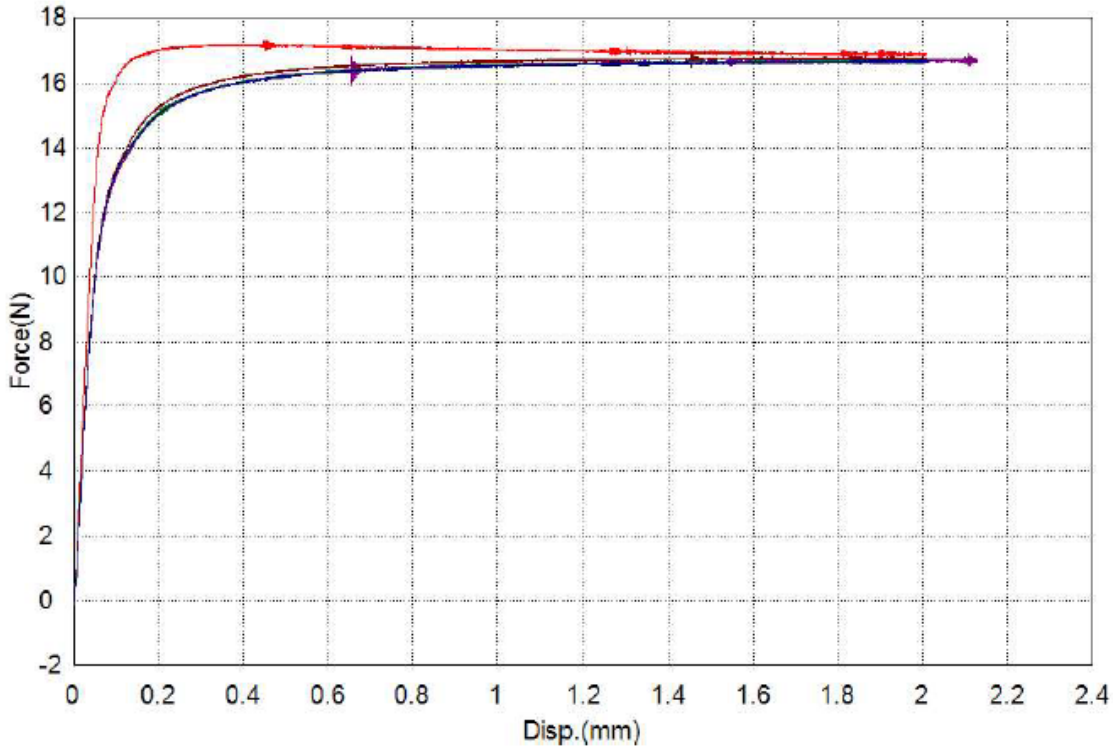

Figure 26. Control Test 2 (5 Cycles)

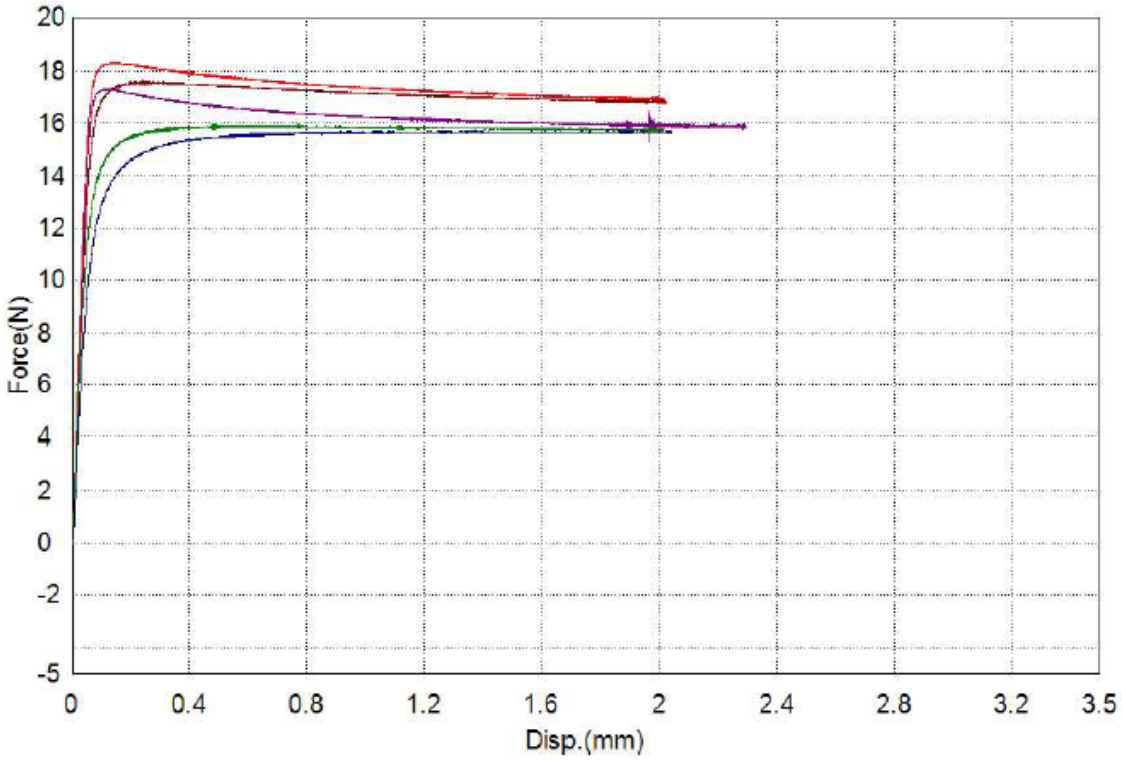

Figure 27. Control Test 3 (5 Cycles)

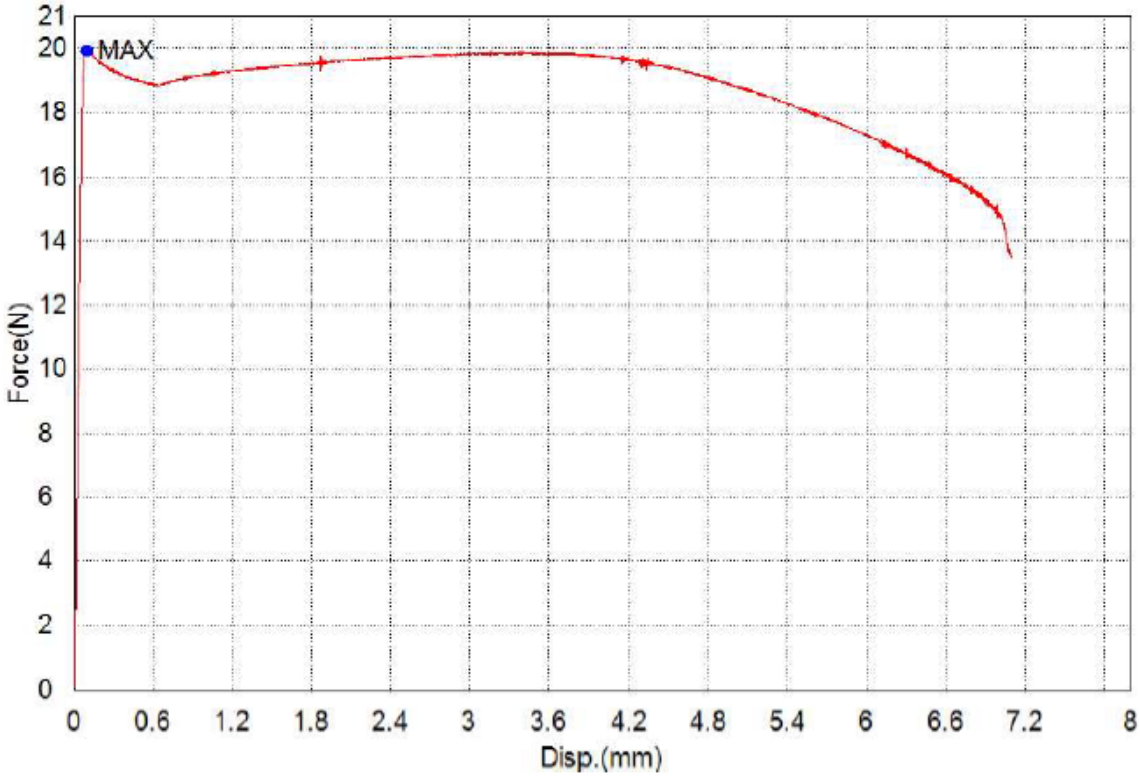

Figure 28. Repulsion Test 1 (1 Cycle, 1 Inch Initial Separation)

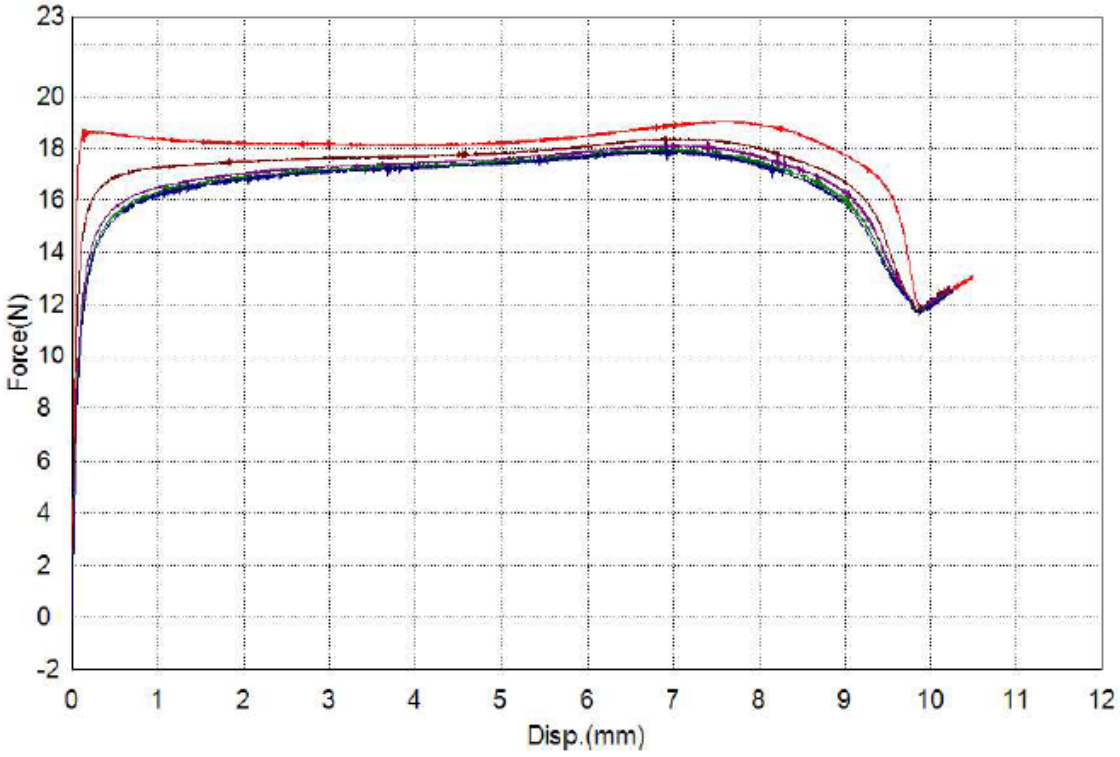

Figure 29. Repulsion Test 2 (5 Cycles, 1 Inch Initial Separation)

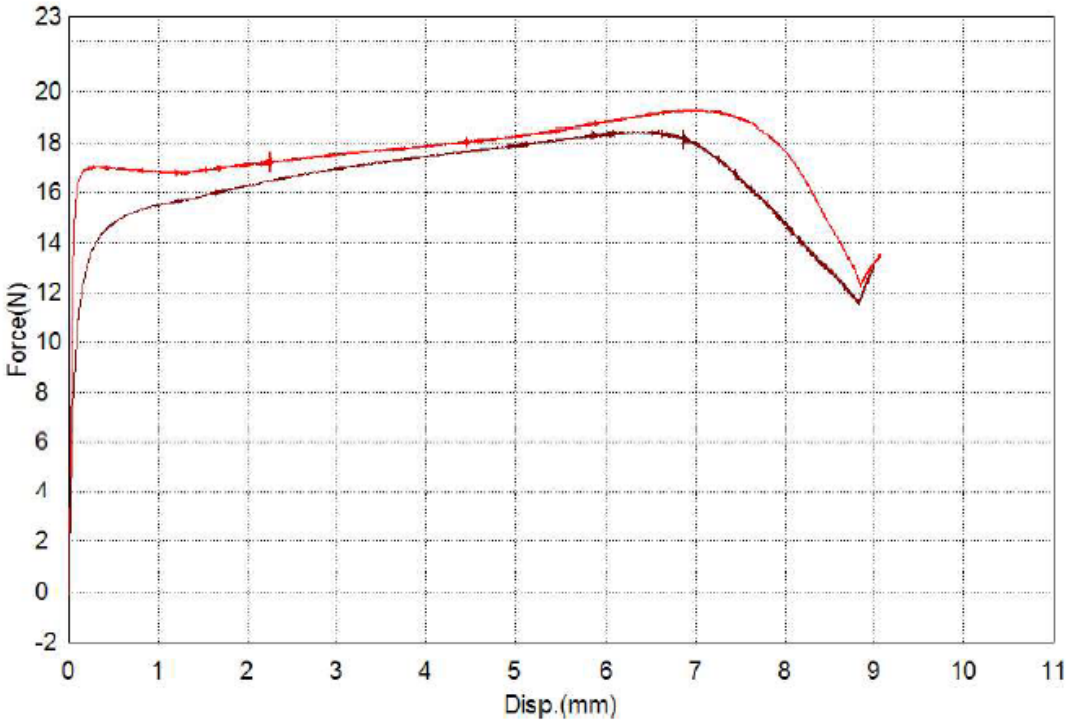

Figure 30. Repulsion Test 3 (2 cycles, 1 Inch Initial Separation)

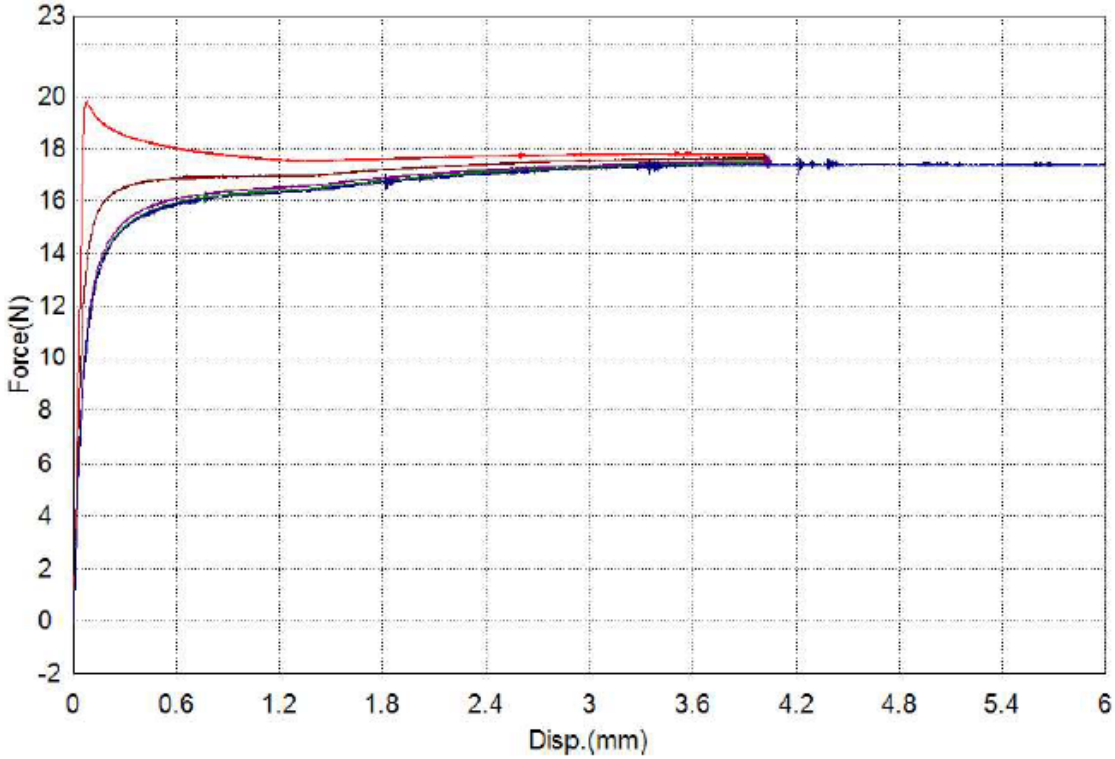

Figure 31. Repulsion Test 4 (5 Cycles, ½" Inch Initial Separation). Forced buckling direction so no late magnetic interactions

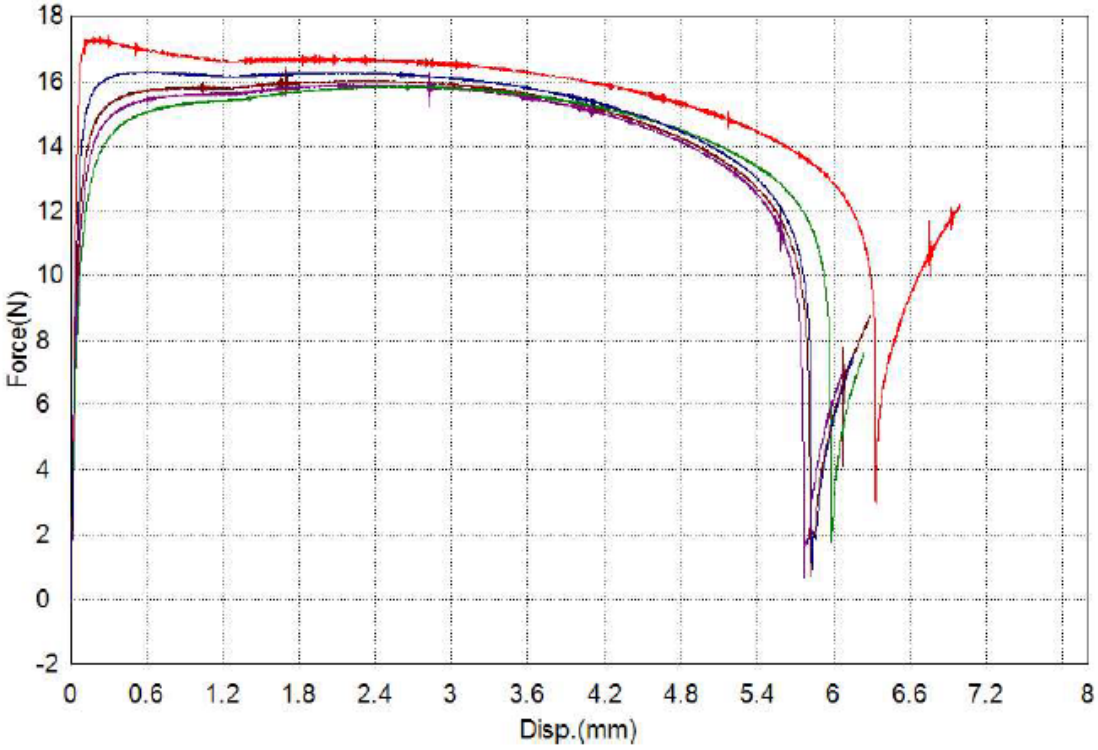

Figure 32. Attraction Test 1 (5 cycles, 1 Inch Initial Separation)

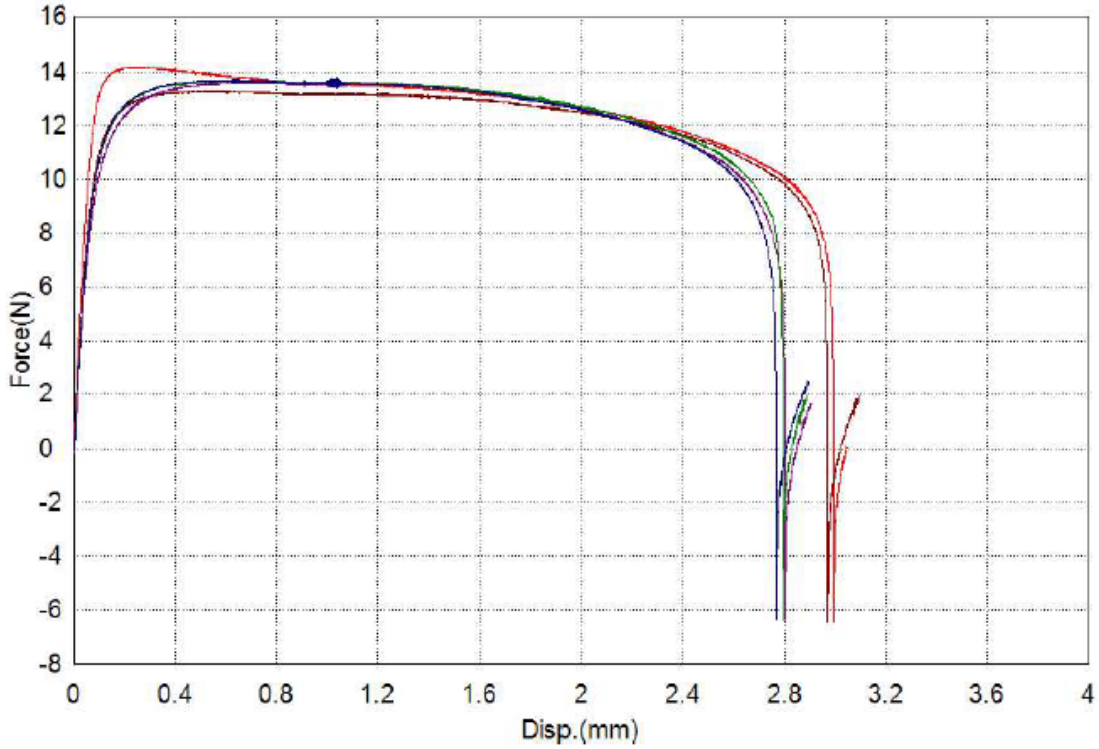

Figure 33. Attraction Test 2 (5 Cycles, ½ Inch Initial Separation)

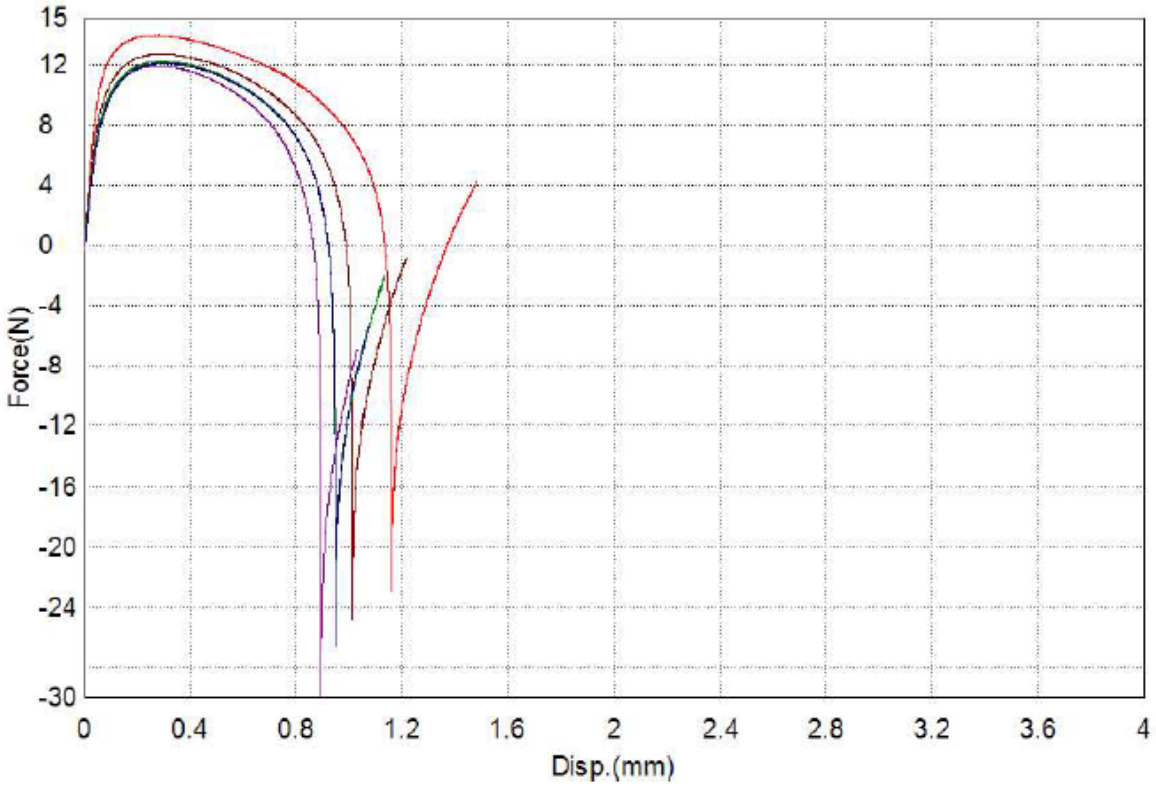

Figure 34. Attraction Test 3 (5 Cycles, ½ Inch Separation)

Appendix B

Raw Data Tables

Table 8. Control Test 1 (1 Cycle) Data

Name	LASE1_Force	LASE2_Force	Max_Force	Max_Stress
Parameters	Stroke 1 mm	Stroke 5 mm	Calc. at Entire Areas	Calc. at Entire Areas
Unit	N	N	N	N/mm2
1 _ 1	17.0598	-.-	19.0018	0.74810
Average	17.0598	-.-	19.0018	0.74810
Standard Deviation	-.-	-.-	-.-	-.-
Range	0.00000	-.-	0.00000	0.00000

Name	Max_Stroke	Break_Force	Break_Stroke_Strain	Energy1
Parameters	Calc. at Entire Areas	Sensitivity: 10	Sensitivity: 10	Start Test - Disp. 2 mm
Unit	mm	N	%	J
1 _ 1	0.08257	-.-	-.-	0.03403
Average	0.08257	-.-	-.-	0.03403
Standard Deviation	-.-	-.-	-.-	-.-
Range	0.00000	-.-	-.-	0.00000

Table 9. Control Test 2 (5 Cycles) Data

Name	LASE1_Force	LASE2_Force	Max_Force	Max_Stress
Parameters	Stroke 1 mm	Stroke 5 mm	Calc. at Entire Areas	Calc. at Entire Areas
Unit	N	N	N	N/mm2
1 _ 1	17.0565	-.-	17.3168	0.68176
1 _ 1	16.6786	-.-	16.9123	0.66584
1 _ 1	16.5640	-.-	16.9315	0.66660
1 _ 1	16.5618	-.-	16.7624	0.65994
1 _ 1	16.5343	-.-	16.7403	0.65907
Average	16.6790	-.-	16.9327	0.66664
Standard Deviation	0.21818	-.-	0.23128	0.00910
Range	0.52220	-.-	0.57650	0.02269

Name	Max_Stroke	Break_Force	Break_Stroke_Strain	Energy1
Parameters	Calc. at Entire Areas	Sensitivity: 10	Sensitivity: 10	Start Test - Disp. 2 mm
Unit	mm	N	%	J
1 _ 1	0.44847	-.-	-.-	0.03343
1 _ 1	1.45377	-.-	-.-	0.03216
1 _ 1	2.10847	-.-	-.-	0.03191
1 _ 1	1.96877	-.-	-.-	0.03190
1 _ 1	1.89740	-.-	-.-	0.03188
Average	1.57538	-.-	-.-	0.03226
Standard Deviation	0.67590	-.-	-.-	0.00067
Range	1.66000	-.-	-.-	0.00155

Table 10. Control Test 3 (5 cycles) Data

Name Parameters Unit	LASE1_Force Stroke 1 mm N	LASE2_Force Stroke 5 mm N	Max_Force Calc. at Entire Areas N	Max_Stress Calc. at Entire Areas N/mm2
1 _ 1	17.3602	-.-	18.3209	0.72129
1 _ 1	17.1567	-.-	17.6422	0.69457
1 _ 1	16.2667	-.-	17.3076	0.68140
1 _ 1	15.8583	-.-	16.0050	0.63012
1 _ 1	15.6539	-.-	15.7525	0.62018
Average	16.4592	-.-	17.0056	0.66951
Standard Deviation	0.76566	-.-	1.09521	0.04311
Range	1.70630	-.-	2.56840	0.10111

Name Parameters Unit	Max_Stroke Calc. at Entire Areas mm	Break_Force Sensitivity: 10 N	Break_Stroke_Strain Sensitivity: 10 %	Energy1 Start Test - Disp. 2 mm J
1 _ 1	0.14830	-.-	-.-	0.03441
1 _ 1	0.23957	-.-	-.-	0.03374
1 _ 1	0.11383	-.-	-.-	0.03226
1 _ 1	0.47880	-.-	-.-	0.03096
1 _ 1	1.86293	-.-	-.-	0.03028
Average	0.56869	-.-	-.-	0.03233
Standard Deviation	0.73741	-.-	-.-	0.00176
Range	1.74910	-.-	-.-	0.00413

Table 11. Repulsion Test 1 (1 Cycle, 1 Inch Initial Separation) Data

Name Parameters Unit	LASE1_Force Stroke 1 mm N	LASE2_Force Stroke 5 mm N	Max_Force Calc. at Entire Areas N	Max_Stress Calc. at Entire Areas N/mm2
1 _ 1	19.1733	18.8156	19.9231	0.78437
Average	19.1733	18.8156	19.9231	0.78437
Standard Deviation	-.-	-.-	-.-	-.-
Range	0.00000	0.00000	0.00000	0.00000

Name Parameters Unit	Max_Stroke Calc. at Entire Areas mm	Break_Force Sensitivity: 10 N	Break_Stroke_Strain Sensitivity: 10 %	Energy1 Calc. at Entire Areas J
1 _ 1	0.09590	-.-	-.-	0.13259
Average	0.09590	-.-	-.-	0.13259
Standard Deviation	-.-	-.-	-.-	-.-
Range	0.00000	-.-	-.-	0.00000

Table 12. Repulsion Test 2 (5 cycles, 1 Inch Initial Separation) Data

Name Parameters Unit	LASE1_Force Stroke 1 mm N	LASE2_Force Stroke 5 mm N	Max_Force Calc. at Entire Areas N	Max_Stress Calc. at Entire Areas N/mm2
1 _ 1	18.3549	18.2112	19.0330	0.74933
1 _ 1	17.2694	17.7960	18.4822	0.72765
1 _ 1	16.4930	17.5912	18.2964	0.72033
1 _ 1	16.2815	17.4138	18.0070	0.70894
1 _ 1	16.2093	17.3887	18.2430	0.71823
Average	16.9216	17.6802	18.4123	0.72490
Standard Deviation	0.90500	0.33883	0.38617	0.01520
Range	2.14560	0.82250	1.02600	0.04039

Name Parameters Unit	Max_Stroke Calc. at Entire Areas mm	Break_Force Sensitivity: 10 N	Break_Stroke_Strain Sensitivity: 10 %	Energy1 Start Test – Disp. 9.5 mm J
1 _ 1	7.68613	-.-	-.-	0.17355
1 _ 1	6.90940	-.-	-.-	0.16596
1 _ 1	7.41090	-.-	-.-	0.16182
1 _ 1	6.87107	-.-	-.-	0.16006
1 _ 1	6.92417	-.-	-.-	0.15924
Average	7.16033	-.-	-.-	0.16413
Standard Deviation	0.36799	-.-	-.-	0.00587
Range	0.81506	-.-	-.-	0.01431

Table 13. Repulsion Test 3 (2 Cycles, 1 Inch Initial Separation) Data

Name Parameters Unit	LASE1_Force Stroke 1 mm N	LASE2_Force Stroke 5 mm N	Max_Force Calc. at Entire Areas N	Max_Stress Calc. at Entire Areas N/mm2
1 _ 1	16.8286	18.2527	19.2719	0.75873
1 _ 1	15.5036	17.8684	18.4973	0.72824
Average	16.1661	18.0606	18.8846	0.74349
Standard Deviation	0.93692	0.27174	0.54773	0.02156
Range	1.32500	0.38430	0.77460	0.03049

Name Parameters Unit	Max_Stroke Calc. at Entire Areas mm	Break_Force Sensitivity: 10 N	Break_Stroke_Strain Sensitivity: 10 %	Energy1 Start Test – Disp. 11 mm J
1 _ 1	6.97980	-.-	-.-	-.-
1 _ 1	6.52020	-.-	-.-	-.-
Average	6.75000	-.-	-.-	-.-
Standard Deviation	0.32499	-.-	-.-	-.-
Range	0.45960	-.-	-.-	-.-

Table 14. Repulsion Test 4 (5 cycles, ½ Inch Initial Separation) Data

Name Parameters Unit	LASE1_Force Stroke 1 mm N	LASE2_Force Stroke 5 mm N	Max_Force Calc. at Entire Areas N	Max_Stress Calc. at Entire Areas N/mm2
1 _ 1	17.6688	-.-	19.8140	0.78008
1 _ 1	16.9293	-.-	17.8126	0.70128
1 _ 1	16.4381	-.-	17.7466	0.69869
1 _ 1	16.3172	-.-	17.5471	0.69083
1 _ 1	16.2319	17.4320	17.6431	0.69461
Average	16.7171	17.4320	18.1127	0.71310
Standard Deviation	0.59665	-.-	0.95642	0.03765
Range	1.43690	0.00000	2.26690	0.08925

Name Parameters Unit	Max_Stroke Calc. at Entire Areas mm	Break_Force Sensitivity: 10 N	Break_Stroke_Strain Sensitivity: 10 %	Energy1 Start Test - Disp. 4 mm J
1 _ 1	0.07447	-.-	-.-	0.07081
1 _ 1	4.00953	-.-	-.-	0.06801
1 _ 1	4.02823	-.-	-.-	0.06617
1 _ 1	3.77723	-.-	-.-	0.06571
1 _ 1	4.21780	-.-	-.-	0.06549
Average	3.22145	-.-	-.-	0.06724
Standard Deviation	1.76614	-.-	-.-	0.00223
Range	4.14333	-.-	-.-	0.00532

Table 15. Attraction Test 1 (5 Cycles, 1 Inch Initial Separation) Data

Name Parameters Unit	LASE1_Force Stroke 1 mm N	LASE2_Force Stroke 5 mm N	Max_Force Calc. at Entire Areas N	Max_Stress Calc. at Entire Areas N/mm2
1 _ 1	16.7455	15.0682	17.4459	0.68685
1 _ 1	15.8153	13.8450	16.4638	0.64818
1 _ 1	15.6034	13.7206	16.2778	0.64086
1 _ 1	15.3549	14.1913	15.9187	0.62672
1 _ 1	16.2172	14.0616	16.3091	0.64209
Average	15.9473	14.1773	16.4831	0.64894
Standard Deviation	0.54695	0.53063	0.57409	0.02260
Range	1.39060	1.34760	1.52720	0.06013

Name Parameters Unit	Max_Stroke Calc. at Entire Areas mm	Break_Force Sensitivity: 10 N	Break_Stroke_Strain Sensitivity: 10 %	Energy1 Start Test - Disp. 6 mm J
1 _ 1	0.28827	-.-	-.-	0.09590
1 _ 1	1.69063	-.-	-.-	0.08758
1 _ 1	2.82547	-.-	-.-	0.08626
1 _ 1	2.65013	-.-	-.-	0.08818
1 _ 1	2.59973	-.-	-.-	0.08955
Average	2.01085	-.-	-.-	0.08949
Standard Deviation	1.05935	-.-	-.-	0.00377
Range	2.53720	-.-	-.-	0.00964

Table 16. Attraction Test 2 (5 cycles, ½ Inch Initial Separation) Data

Name	LASE1_Force	LASE2_Force	Max_Force	Max_Stress
Parameters	Stroke 1 mm	Stroke 5 mm	Calc. at Entire Areas	Calc. at Entire Areas
Unit	N	N	N	N/mm2
1 _ 1	13.5786	-.-	14.1707	0.55790
1 _ 1	13.1623	-.-	13.2917	0.52329
1 _ 1	13.5353	-.-	13.6274	0.53651
1 _ 1	13.5993	-.-	13.6706	0.53821
1 _ 1	13.5730	-.-	13.7784	0.54246
Average	13.4897	-.-	13.7078	0.53967
Standard Deviation	0.18448	-.-	0.31633	0.01246
Range	0.43700	-.-	0.87900	0.03461

Name	Max_Stroke	Break_Force	Break_Stroke_Strain	Energy1
Parameters	Calc. at Entire Areas	Sensitivity: 10	Sensitivity: 10	Start Test - Disp. 3 mm
Unit	mm	N	%	J
1 _ 1	0.22913	1.61489	1.49632	0.03745
1 _ 1	0.60310	1.47009	1.48457	0.03592
1 _ 1	0.95357	1.42415	1.40037	-.-
1 _ 1	0.67407	1.77113	1.39570	-.-
1 _ 1	1.04070	2.02179	1.38280	-.-
Average	0.70011	1.66041	1.43195	0.03669
Standard Deviation	0.32100	0.24340	0.05394	0.00108
Range	0.81157	0.59764	0.11352	0.00153

Table 17. Attraction Test 3 (5 cycles, ½ Inch Initial Separation) Data

Name	LASE1_Force	LASE2_Force	Max_Force	Max_Stress
Parameters	Stroke 1 mm	Stroke 5 mm	Calc. at Entire Areas	Calc. at Entire Areas
Unit	N	N	N	N/mm2
1 _ 1	7.44184	-.-	13.9616	0.54967
1 _ 1	-2.3669	-.-	12.7236	0.50093
1 _ 1	-9.1465	-.-	11.9284	0.46962
1 _ 1	-11.351	-.-	12.2390	0.48185
1 _ 1	-11.074	-.-	12.1123	0.47686
Average	-5.2993	-.-	12.5930	0.49579
Standard Deviation	7.99542	-.-	0.81979	0.03228
Range	18.7928	-.-	2.03320	0.08005

Name	Max_Stroke	Break_Force	Break_Stroke_Strain	Energy1
Parameters	Calc. at Entire Areas	Sensitivity: 10	Sensitivity: 10	Start Test - Disp. 1 mm
Unit	mm	N	%	J
1 _ 1	0.26430	-11.279	0.58005	0.01180
1 _ 1	0.30197	-11.692	0.50620	0.00989
1 _ 1	0.26913	-13.429	0.44667	0.00635
1 _ 1	0.28263	-12.285	0.47332	0.00796
1 _ 1	0.31030	-11.983	0.47353	0.00788
Average	0.28567	-12.134	0.49595	0.00878
Standard Deviation	0.02007	0.81379	0.05153	0.00211
Range	0.04600	2.15000	0.13338	0.00545

BIBLIOGRAPHY

1. Lammers, A., & Zurcher, U. (2011). Torque around the center of mass: dynamic stability during quadrupedal arboreal locomotion in the Siberian chipmunk (Tamias sibiricus). *Zoology*, *114*(2), 95-103. http://dx.doi.org/10.1016/j.zool.2010.11.004

2. Harne, R., & Wang, K. (2013). A review of the recent research on vibration energy harvesting via bistable systems. *Smart Materials And Structures*, *22*(2), 023001. http://dx.doi.org/10.1088/0964-1726/22/2/023001

3. Crivaro, A., Sheridan, R., Frecker, M., Simpson, T. W., & Von Lockette, P. (2015). Bistable compliant mechanism using magneto active elastomer actuation. *Journal of Intelligent Material Systems and Structures*, *27*(15), 2049–2061. doi:10.1177/1045389x15620037

4. Zhao, J., Huang, Y., Yang, Y., & Gao, R. (2012). Dynamics of a novel bistable mechanism with mechanical-magnetic coupled structure. *Journal Of Central South University*, *19*(7), 1853-1858. http://dx.doi.org/10.1007/s11771-012-1219-7

5. Jianguo, C., Xiaowei, D., Ya, Z., Jian, F., & Yongming, T. (2015). Bistable Behavior of the Cylindrical Origami Structure With Kresling Pattern. *Journal Of Mechanical Design*, *137*(6), 061406. http://dx.doi.org/10.1115/1.4030158

6. Norman, A., Seffen, K., & Guest, S. (2008). Multistable corrugated shells. *Proceedings Of The Royal Society A: Mathematical, Physical And Engineering Sciences*, *464*(2095), 1653-1672. http://dx.doi.org/10.1098/rspa.2007.0216

7. Kebadze, E., Guest, S., & Pellegrino, S. (2004). Bistable prestressed shell structures. *International Journal Of Solids And Structures*, *41*(11-12), 2801-2820. http://dx.doi.org/10.1016/j.ijsolstr.2004.01.028

8. Schultz, M. (2008). A Concept for Airfoil-like Active Bistable Twisting Structures. *Journal Of Intelligent Material Systems And Structures*, *19*(2), 157-169. http://dx.doi.org/10.1177/1045389x06073988

9. Rossiter, J., Stoimenov, B., & Mukai, T. (2006). A Self-switching Bistable Artificial Muscle Actuator. *2006 SICE-ICASE International Joint Conference*. http://dx.doi.org/10.1109/sice.2006.315374

10. Budynas, R. G. (1998). *Advanced strength and applied stress analysis* (2nd ed.). Boston: McGraw Hill Higher Education.

11. Wang, C., Reddy, J. N., & Wang, C. Y. (2005). Exact solutions for buckling of structural members. Boca Raton, Fla.: CRC press.

12. Yung, K. W., Landecker, P. B., & Villani, D. D. (1998). An analytic solution for the force between Two magnetic dipoles. *Magnetic and Electrical Separation*, *9*(1), 39–52. doi:10.1155/1998/79537

13. *Polymethylmethacrylate (PMMA, Acrylic) :: MakeItFrom.com*. (2017). *Makeitfrom.com*. Retrieved 2 March 2017, from http://www.makeitfrom.com/material-properties/Polymethylmethacrylate-PMMA-Acrylic/

14. *K&J Magnetics: B444*. (2017). *Kjmagnetics.com*. Retrieved 15 March 2017, from http://www.kjmagnetics.com/proddetail.asp?prod=B444

ACADEMIC VITA

Daniel T. Murt

dtmurt@gmail.com • linkedin.com/in/danielmurt

EDUCATION:

The Pennsylvania State University, University Park, PA
Bachelor of Science in Mechanical Engineering, May 2017
Minor in Mathematics
Schreyer Honors College; Dean's List

Relevant Courses: Finite Element Analysis; Optics/Quantum Mechanics; Engineering Thermodynamics; Manufacturing Processes; Circuit Analysis and Power Distribution; Strength of Materials; Differential Equations/Calculus 1, 2, and 3; Material Properties

EXPERIENCE:

Mechanical Engineering Co-Op at Burns Engineering Inc. **Summer 2016**

- Worked successfully with a team of engineers on the implementation of Positive Train Control (PTC) technology to make railroads safer for clients including AMTRAK, The Alaska Railroad, SEPTA, and The Massachusetts Bay Transportation Authority (MBTA)
- Effectively implemented the QA/QC process by revising, checking, and finalizing signals engineering drawings and signals software to be used to monitor and control trains
- Extensively utilized AutoCAD and Excel functions to organize, update, and publish engineering blueprints and drawings to customer specifications
- Assisted in the redesign of signals engineering systems and assemblies used in PTC

Engineering Intern at ESI Equipment **Summer 2015**

- Drafted, revised, and digitally stored employer catalog of manufactured parts used in emergency response vehicles
- Designed slide tray mounts and in-door glove box storage assemblies for use in ambulances and in SPACEKAP units
- Created sheet metal specifications for the fabrication of new parts important to the functionality of Rapid Response Emergency Units
- Conducted virtual simulations of assemblies consisting of personally-designed parts in a CAD environment

Engineering Intern at NAVMAR Applied Sciences **Summer 2014**

- Designed and oversaw the fabrication of a prototype TDI camera mount for a wide area digital surveillance payload on a Tigershark UAV
- Collaborated with other engineering professionals on a variety of projects relating to the improvement of current military UAV capabilities
- Conducted numerous concept tests with RC aircraft including remote quadcopters and model jets
- Worked extensively with 3D printing technology (Makerbot Replicator 2/2x/Z18, Stratasys Mojo) to model, create and test CAD prototype designs
- Used industry standard sheet metal working processes including the practical application of metal fasteners, as well as the creation of usable engineering prints

SKILLS:

Extensive experience with CAD programs including AutoCAD, SolidWorks, and FreeCAD; Proficient in the MATLAB programming language; Proficient in Abaqus (FEA); Advanced knowledge of Microsoft Office (Excel, Word, PowerPoint), Adobe Acrobat, and Bluebeam Revu; Proficient in electrical soldering; Basic knowledge of German

ACTIVITIES:

Resident Assistant; Tau Beta Pi Engineering Honor Society Member**;** Vice President of Upper Moreland Interact Service Club; National Honor Society and German Honor Society Member; Penn State eSports Member; Amateur Radio Technician; Guitarist (Competitive Jazz/Classical)